JOURNAL OF GEOPHYSICAL RESEARCH, VOL. 89, NO. A10, PAGES 8885–8906, OCTOBER 1, 1984

Particle and Field Characteristics of the High-Latitude Plasma Sheet Boundary Layer

G. K. PARKS,[1] M. MCCARTHY,[1] R. J. FITZENREITER,[2] J. ETCHETO,[3] K. A. ANDERSON,[4] R. R. ANDERSON,[5] T. E. EASTMAN,[5] L. A. FRANK,[5] D. A. GURNETT,[5] C. HUANG,[5] R. P. LIN,[4] A. T. Y. LUI,[6] K. W. OGILVIE,[2] A. PEDERSEN,[7] H. REME,[8] AND D. J. WILLIAMS[6]

Particle and field data obtained by eight ISEE spacecraft experiments are used to define more precisely the characteristics of the high-latitude boundary region of the plasma sheet. We find that there is a region immediately adjacent to the high-latitude plasma sheet boundary whose particle and field characteristics are distinctly different from its neighbors, the lobe and the plasma sheet. This region supports intense ion flows, field-aligned currents, large amplitude electric fields, and enhanced broad band electrostatic noise. A detailed analysis of events detected on April 19, 1978, shows that the plasma distributions in the region are unstable. For instance, bidirectional field-aligned electron distributions are observed at nearly all energies (a few electron volts to a few hundred keV). Both the differential energy spectra and the reduced distribution function $F(v_{\|}) = 2\pi\int v_{\perp} f(v_{\|}, v_{\perp}) dv_{\perp}$ show significant peaks at 100–400 eV. These peaks comprise electrons coming from the earthward direction. Ions below a few keV are convected in the direction perpendicular to **B**, whereas the higher energy ions (>30 keV) are field-aligned and travelling mainly toward the earth. The electric field in the region is intense, spiky, and possibly time varying. The magnetic B_y component increases dramatically from a few nanoteslas to more than 20 nT, indicating presence of a field-aligned current. These features are in contrast with the plasma characteristics outside the region. In the adjacent regions (closer to the lobe and the inner plasma sheet regions), the electron distributions are nearly isotropic. Ion flow is virtually at a standstill. The high-energy ions (>30 keV) are anisotropic and field-aligned but bidirectional.

1. INTRODUCTION

It is becoming increasingly evident that the neighborhood of the high-latitude boundary of the plasma sheet supports a considerable amount of particle and field activities. *Fairfield* [1973] deduced from magnetometer data the existence of current sheets near the plasma sheet boundary. *Scarf et al.* [1974] and *Gurnett et al.* [1976] showed that although electromagnetic and electrostatic waves are detected throughout the distant geomagnetic tail, the amplitude of the broadband electrostatic waves is enhanced across the plasma sheet boundary. *Lui et al.* [1977] observed high-speed ion flows as the spacecraft crossed the plasma sheet boundary, and *DeCoster and Frank* [1979] showed that such high-speed ion flows are detected primarily in the area adjacent to the high-latitude plasma sheet boundary. Recent ISEE experiments have complemented and expanded these earlier observations. *Parks et al.* [1979] identified a particle region immediately adjacent to the high-latitude plasma sheet boundary. *Cattell et al.* [1982] then showed that intense electric fields exist in this region. Large-amplitude electric field has also been observed by *Aggson et al.* [1983]. Nonthermal ion layers [*Mobius et al.*, 1980], energetic ion beams [*Williams*, 1981], and field-aligned currents [*Frank et al.*, 1981] are also confined to the outer edge of the plasma sheet boundary. *Spjeldvik and Fritz* [1981] studied the flow characteristics and deduced that the flow layer was of the order of ~2 ion gyroradii thickness. *Eastman et al.* [1984] studied ion flow characteristics in conjunction with ion composition measurements and concluded, as did *Peterson et al.* [1981] that ionospheric oxygen exists near the plasma sheet boundary.

These results come from different experiments flown through different parts of the plasma sheet at different times. Although all of these observations made references to the high-latitude boundary of the plasma sheet, the relative location where each particle or field phenomenon occurred is not precisely known. This ambiguity exists because the term "plasma sheet boundary layer" has been defined in each case by the particular instrument making the observation and there has not yet been a systematic study that attempts to interrelate the various phenomena. It is important to define clearly where each phenomenon occurs relative to other phenomena.

The first step toward resolving this problem is to coordinate the various observations. The purpose of this paper is to present and discuss particle and field data that were obtained by eight complementary experiments flown on the ISEE spacecraft. We will use correlated features observed on April 19, 1978, to define and characterize in as much detail as possible the particle and field features in the neighborhood of the plasma sheet boundary. (Note that the proton and alpha particle energy spectra on this day at 1500 UT have also been studied by *Ipavich and Scholer* [1983]. Their results come from deeper in the plasma sheet, whereas our results, to be reported here, come from the region of the plasma sheet boundary.) See *Eastman et al.* [1983] for ion flow details observed around 1300 UT. Our data set includes electrons and ions from a few electron volts to several hundred keV [*Anderson et al.*, 1978; *Frank et al.*, 1978; *Ogilvie et al.*, 1978; *Williams et al.*, 1978], magnetic [*Russell*, 1978], and electric fields [*Mozer et al.*, 1978] and waves [*Gurnett et al.*, 1978; *Harvey et al.*, 1978]. This data set will show that the behavior of parti-

[1] Geophysics Program, University of Washington, Seattle.
[2] NASA Goddard Space Flight Center, Greenbelt, Maryland.
[3] Centre de Recherches sur la Physique de l'Environnement, Centre National d'Etudes des Télécommunications, Issy les Moulineaux, France.
[4] Space Sciences Laboraotry, University of California, Berkeley.
[5] Physics Department, University of Iowa, Iowa City.
[6] Applied Physics Laboratory, Johns Hopkins University, Laurel, Maryland.
[7] Space Science Department, European Space Agency, Noordwijk, The Netherlands.
[8] Centre d'Etude Spatiale des Rayonnements, Université Paul Sabatier, Toulouse, France.

Paper number 4A0833.
0148-0227/84/004A-0833$05.00

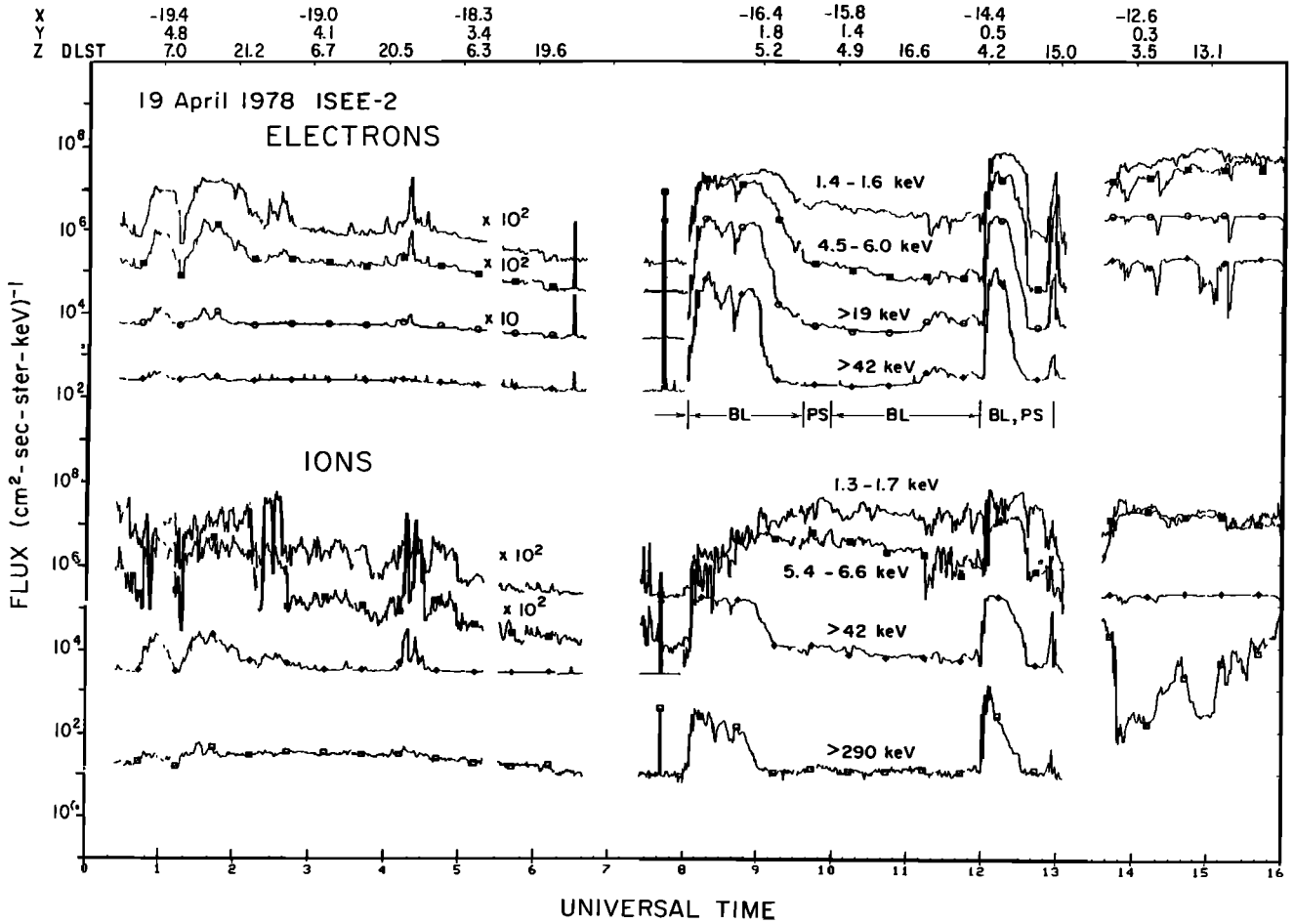

Fig. 1. Electron and ion fluxes at several fixed energies plotted as a function of universal time during an ISEE 2 inbound pass. Variations of fluxes are observed in time scales of a few minutes to hours. The sharp increase of fluxes at 0800 UT and 1200 UT occurs in association with auroral zone magnetic activities. Note that significant fluxes of lower energy particles remain high while high energy fluxes reduce to background levels.

cles and fields is extremely complicated, and it takes the entire particle and field data set to define precisely the plasma sheet boundary layer. Many of the features are not understood at this time. Consequently, no attempt will be made here to fit the observations to any models (see, for example, *Cowley and Southwood* [1980] for a theoretical model of the geomagnetic tail.)

In sections 2.1 and 2.2 we will introduce the reader to the ISEE data set by use of "coarse" time resolution data so that the data presented in this paper can be compared and related to studies conducted earlier on this subject. High-time resolution data will be shown in section 2.3. This data set permits accurate determination of wave onset times that can be compared to particle onset times and their features. The details of plasma distributions are shown in section 2.4. Summary and discussion follow in section 3.

2. Data Presentation

2.1. *General Behavior of Geomagnetic Tail Particles*

It has been known since 1965 that a spacecraft in the distant geomagnetic tail frequently detects energetic particles during geomagnetic disturbances [*Anderson*, 1965; *Frank*, 1965; *Konradi*, 1966; *Serlemitsos*, 1966]. Typical examples of such particle fluxes detected by the ISEE spacecraft during an inbound pass on April 19, 1978, are shown in Figure 1. The upper four curves show the behavior of electron fluxes and the bottom four the ion fluxes. The data here are 32-s averages, and the particles have fairly large pitch-angles, about 70°–90°. The particles of the geomagnetic tail are dynamic and variations of fluxes from a few minutes to hours are common and frequent. Physical causes responsible for the variations are not all understood at this time. Some of the variations, for instance the increases observed at 0800 UT and 1200 UT, are associated with auroral zone magnetic activities (magnetograms not shown). These increases have rapid onset times of a few minutes or less and decay away in tens of minutes to hours [*Anderson*, 1965]. Note that particles of lower energies have longer durations. (For possible explanation of the temporal behavior at different energies, see *Baker et al.* [1979].) The variations of electrons and ions do not have a simple relationship as demonstrated by the 0800 UT event in which the two low energy ion fluxes behaved very differently from the more energetic ions and electrons.

The behavior of plasma ion density and flow velocities for April 19, 1978 is shown in Figure 2. The data shown here are integrals of the three dimensional ion distributions that are obtained every 128 s in the energy range 1.24 eV to about 44.5 keV. This figure shows that there was a considerable amount of density variation throughout the interval. However, the 0800 UT and the 1200 UT events can be identified in the ion density time profile as abrupt increases of the ion density. At

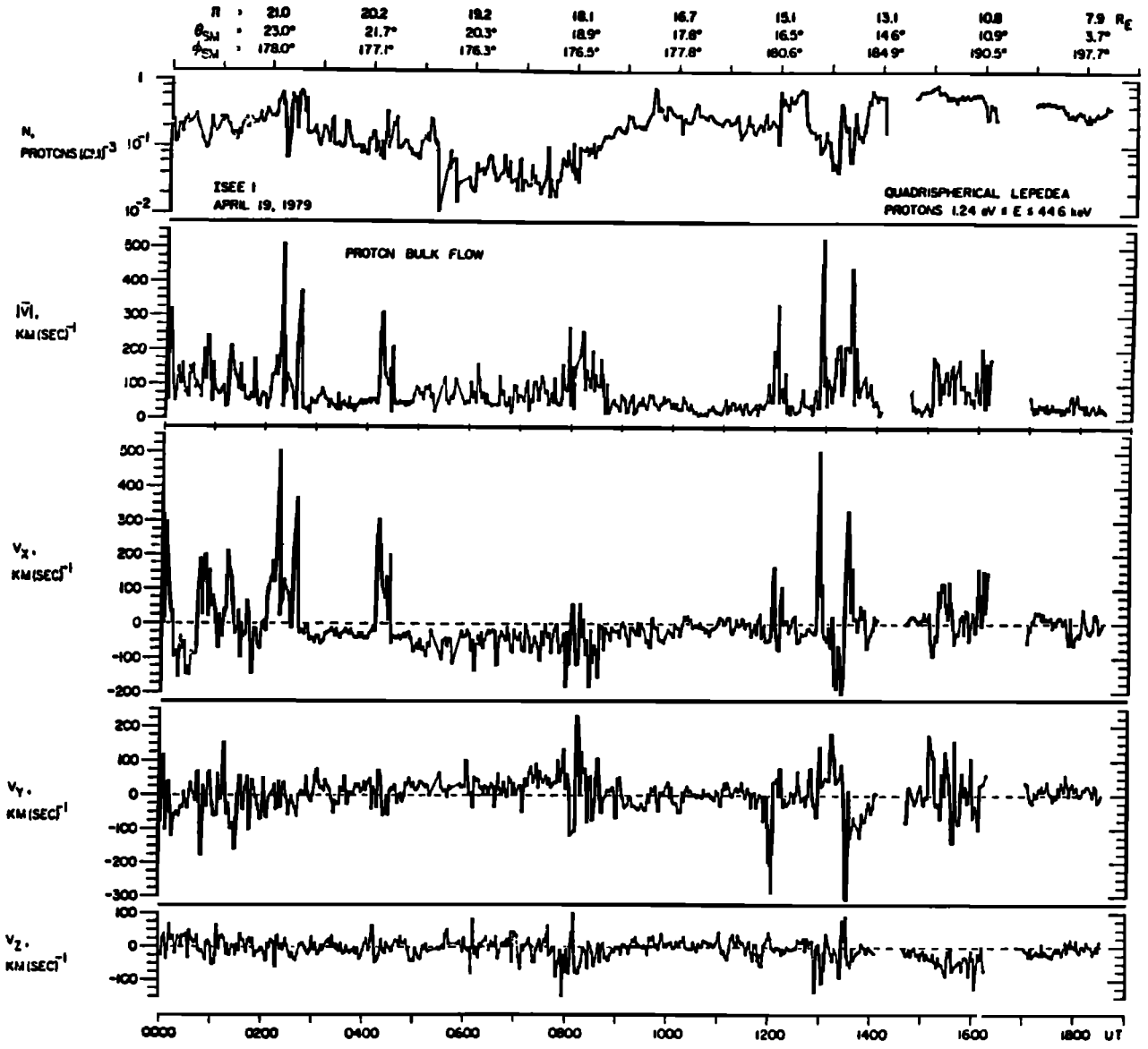

Fig. 2. Plasma ion and flow velocities plotted as a function of universal time. Abrupt increase of flow velocities is detected in conjunction with abrupt density jumps, for example, 0800 UT and 1200 UT. The enhanced flow is observed only during the leading edge of particle increases.

0800 UT, the density increased from about 0.04 to 0.09 ions $(cm)^{-3}$, and at 1200 UT from about 0.3 $(cm)^{-3}$ to 0.7 $(cm)^{-3}$. Large variations of ion density ($\delta n \gtrsim 0.1$) were commonly observed in the interval 0800–1200 UT. These variations suggest that for most of this interval the ISEE 1 spacecraft was in the vicinity of the plasma sheet boundary layer.

The bulk plasma flow was enhanced between 0800 UT and 0840 UT. The flow during this time interval reversed direction several times in all three velocity components, and the maximum flow attained was about 250 km/s. Large flow velocities were recorded mainly in the V_x and V_y components. (The coordinate system here is geocentric solar ecliptic. V_x is positive earthward, V_y positive duskward, and V_z positive toward the ecliptic north.) The plasma was essentially stationary between 0840 UT and 1200 UT. Then significant V_x and $-V_y$ developed ($V_x = 160$ km/s, $V_y = -280$ km/s). This enhanced flow lasted for less than 10 min. Similar to the 0800 UT event, V_x reversed direction here several times, whereas V_y was directed mainly in the dawnward direction. Note that for both 0800 UT and the 1200 UT events, the flow in the Z direction was relatively small (less than 100 km/s). The enhanced flow is observed only during the leading edge of the particle flux increases (Figure 1). The events shown here are similar to those studied by *Lui et al.* [1983] and *DeCoster and Frank* [1979].

2.2. *Waves in the Geomagnetic Tail*

General features of waves observed in the geomagnetic tail and their correlation to electron fluxes are shown in Figure 3. The magnetic wave measurements are detected in 14 discrete frequency channels from 5.6 Hz to 10 kHz (top panel). The electrostatic wave measurements (bottom panel) are detected in 16 discrete frequency channels from 5.6 Hz to 31.1 kHz (311.1 kHz on ISEE 1). The ordinate of the wave data from the base line of one channel to the next channel represents a 100-dB increase in the field strength. For the electrostatic channels, the field strength varies from about 0.1×10^{-6} V/m to 10×10^{-3} V/m. The upper boundary of the dark solid

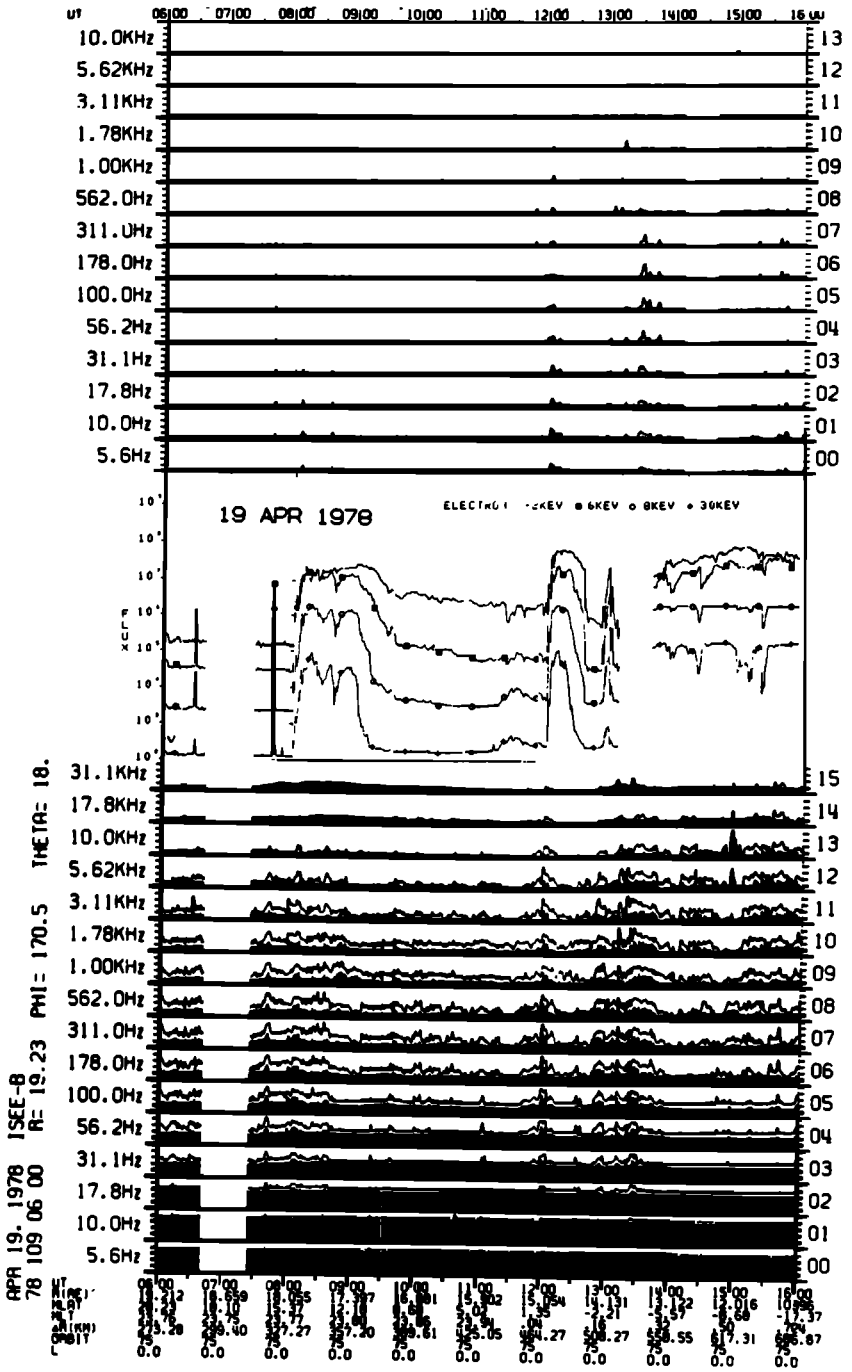

Fig. 3. A 10-hr summary of electron and wave activities. The top panel shows the electromagnetic wave data, the middle panel shows the electron fluxes, and the bottom panel shows the electrostatic wave data. The enhancement of wave activity is primarily associated with the leading edge of particle flux increases.

areas represents the average field strength while the lines above the solid area represent the peak values. Sandwiched in between the two wave data panels are measurements of electron fluxes shown in Figure 1.

The enhanced electrostatic waves were observed for the entire 10-hr interval shown. However, there are several time intervals when the electrostatic wave amplitude is considerably enhanced. The enhanced wave activity is observed in coincidence with increases of particle fluxes, for instance, the events starting around 0740 UT, 0800 UT, 1200 UT, and 1300 UT. Weak but measurable wave activity is also observed in the magnetic channels during these times. The wave activity is enhanced from about 17.8 Hz to about 10 kHz for the electrostatic waves and from about 5.6 Hz to about 178 Hz for the electromagnetic waves. The enhanced wave activity, like the flow, is observed only during the few minutes immediately following the particle onsets (see Figure 2). The electrostatic waves here are the same "broadband electrostatic noise" studied by *Gurnett et al.* [1976]. The electromagnetic waves are the "whistler magnetic noise bursts."

2.3. *High-Time Resolution Particle and Field Data*

The time interval around 1200 UT will now be examined in much more detail. Figures 4*a* and 4*b* show 1/4-s averages of

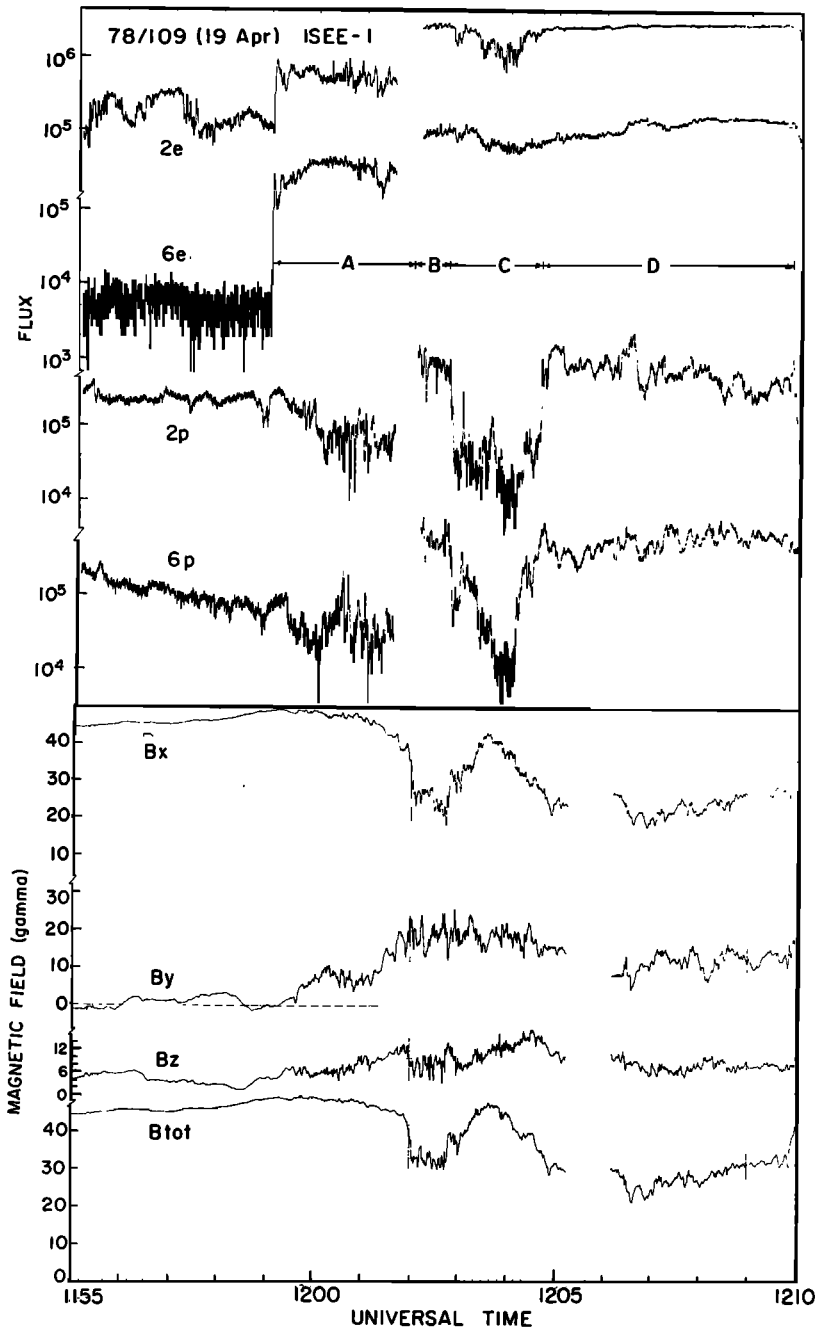

Fig. 4*a*. High-time resolution particle and magnetic field data. The behavior of particle fluxes indicates that there is a region (time intervals A and C) adjacent to the plasma sheet boundary that is different from the plasma sheet and the lobe. The increase of B_y in this region can be interpreted in terms of a field-aligned current.

electron and ion fluxes from the two lowest energy channels of the fixed energy detector system on ISEE 1 together with the magnetic and electric field data (also 1/4-s averages). As mentioned earlier, the particles measured here have pitch angles around 70°–90°. The components of the magnetic and electric field are displayed in the geocentric solar ecliptic coordinate system (GSE). Attention is called to the features of particle fluxes observed in the four time intervals: A (1159–1202 UT), B (1202–1202:50 UT), C (1202:50–1204:40 UT), and D (beyond 1204:40 UT). Fluxes of particles in A and C are similar and lower than those in B and D. This feature is most clearly seen in the ion data. Our data here suggest that the spacecraft upon leaving the lobe (~1159 UT) encountered two different plasma regions. Region A (and C) is bordered on one side by the lobe and on the other side by the plasma sheet (more on this below).

The magnetic field component B_x was nearly at maximum around 1159 UT (note that B_x has been increasing slowly prior to 1159 UT). B_x then began to decrease in time interval A and in coincidence with the recovery of ion fluxes in interval B, a minimum B_x was observed. The correlation of B_x and ion fluxes shows that low ion fluxes are detected with large B_x values and higher fluxes with smaller B_x values. B_y began to increase around 1159 UT. It reached a maximum value of about 20 nT at 1202 UT from about zero at 1159 UT (all in time interval A). B_y remained nearly constant in intervals B

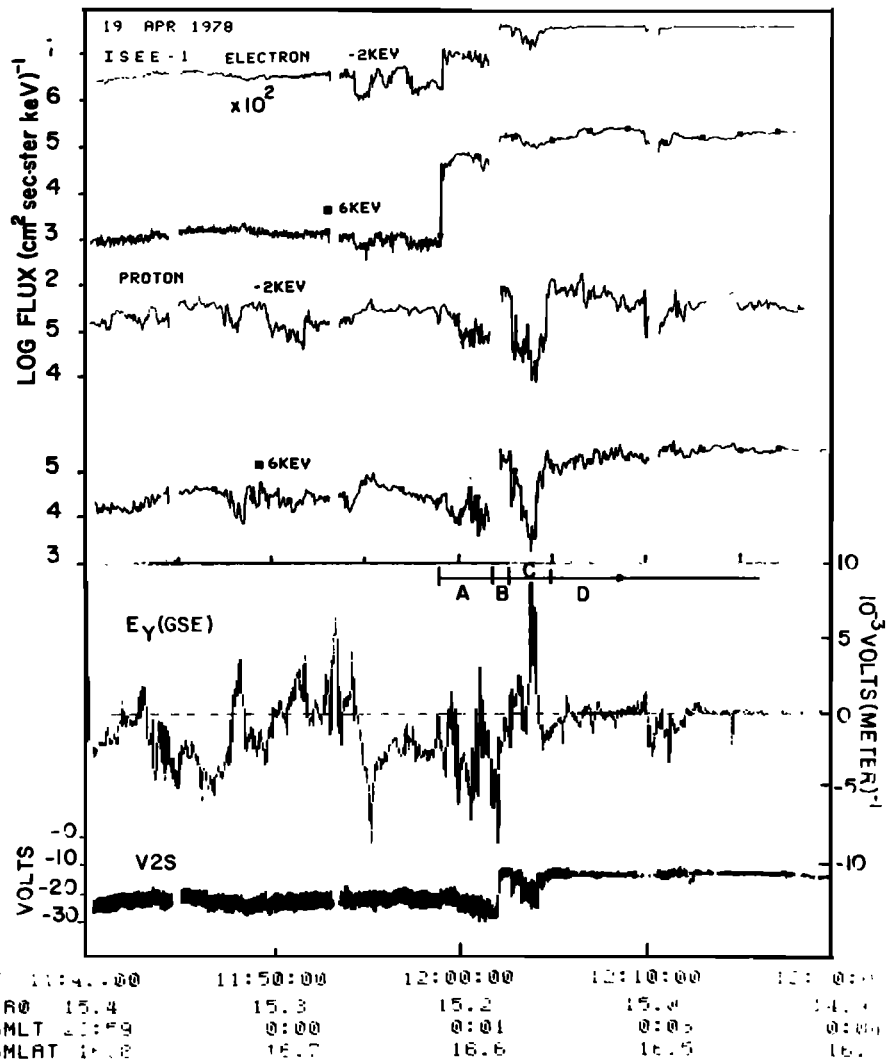

Fig. 4*b*. High-time resolution particle and electric field data. The electric field is spiky and is several millivolts per meter.

and C and decreased to about 15 nT in the remaining intervals. B_y can be interpreted in terms of a field-aligned current. Thus, the field-aligned current was "building" up in interval A, maintained itself through interval C, and subsequently decreased. The B_z component slowly increased from about 5 nT at 1159 UT to about 10–12 nT at 1202 UT. It then decreased abruptly (in interval B) and again slowly increased to about 12 nT by 1205 UT. B_T (total B) generally followed the behavior of B_x.

To interpret the electric field data (Figure 4*b*), note that V2S, which is approximately a measure of negative potential of the spacecraft [*Pedersen et al.*, 1983], is according to Langmuir theory proportional to the logarithm of the density times the square root of electron temperature. V2S shows that prior to 1159 UT, the spacecraft was immersed in a tenuous plasma region and the spacecraft potential was about 20–25 V. Between 1159 UT and 1202 UT, V2S increased by several volts and then abruptly reduced to about 10 V at 1202 UT, which is an indication that the spacecraft temporally entered a region of higher density or higher temperature plasma.

Large variations and enhancement of E_y are observed in the time interval 1159 UT to 1205 UT (time interval A and C) and smaller variations subsequently. Owing to insufficient bias current to the probes, the variations observed before 1202 UT lend themselves only to qualitative interpretation. After this time, E_y is quantitative. For instance, the spike observed in E_y during time interval C is about 5×10^{-3} V/m. At this time interval, $B_x = 44$ nT, $B_y = 20$ nT, and $B_z = 11$ nT. If we now assume that $\mathbf{E} \cdot \mathbf{B} = 0$ and $E_x = 0$ (that is, $E_{\parallel}$ is assumed zero), a value for E_z is obtained to be -8×10^{-3} V/m. $\mathbf{E} \times \mathbf{B}$ velocities computed for these electric field values give $V_x = 96$ km/s and $V_y = -141$ km/s. The behavior of the electric field can be summarized as "spiky," rapidly varying in both magnitude and direction, and possibly time varying. The results obtained here are consistent with plasma ion flow measurements (see Figure 2).

Particles and field signatures indicate that the ISEE spacecraft traversed two different regions of space. The region of space traversed in time intervals A and C is measurably different from the region traversed in time intervals B and D. The higher fluxes encountered in intervals B and D for both electrons and ions suggest that at these times we were probably sampling particles from regions deeper in the plasma sheet. This interpretation will be adopted in this paper. This means during time intervals A and C we sampled regions of space immediately outside the plasma sheet boundary. These separ-

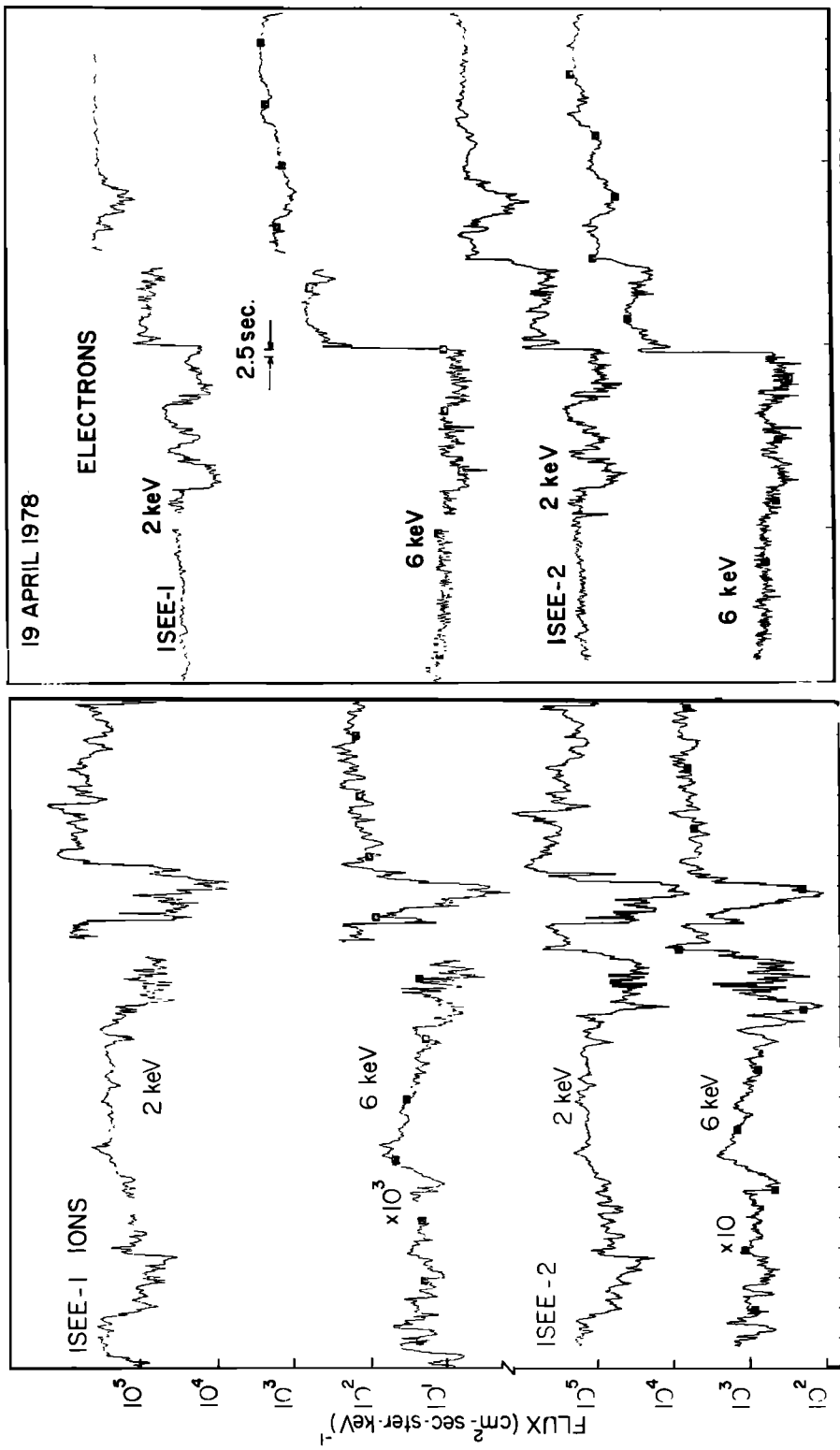

Fig. 5. Behavior of electron fluxes observed on both ISEE 1 and 2 spacecraft. Note the similarities of the features observed. ISEE 2 detected the leading edge by about 2.5 s.

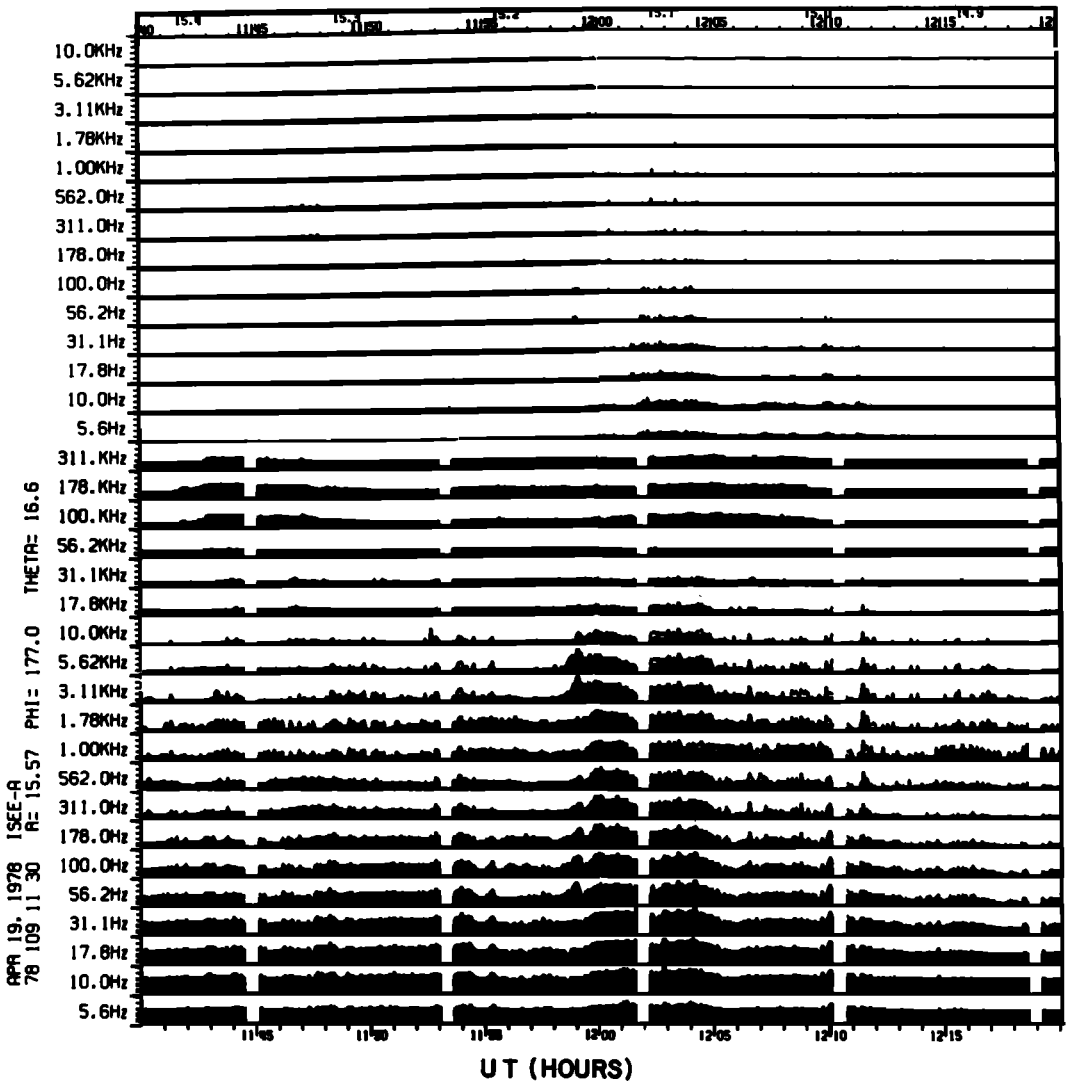

Fig. 6. High-time resolution wave data. The electrostatic waves are enhanced in the frequency interval 5.6 Hz to more than 31.1 kHz. The enhanced waves are observed from 1159 to about 1205 UT. Small bursts of electromagnetic waves are also observed.

ate regions were encountered by both ISEE spacecraft. The electron and ion flux time profiles detected on the two spacecraft are remarkably similar (Figure 5). At 1200 UT, the two spacecraft were separated in X_{GSE} by 413 km with ISEE 1 located further in the tail, in Y_{GSE} by 153 km with ISEE 1 located further toward dawn, and in Z_{GSE} by 145 km with ISEE 1 further from the neutral sheet. The onset of electron flux increases was recorded earlier on ISEE 2 by about 2–2.5 s, which translates to an apparent speed of 70–200 km/s depending on which separation distance is taken. Assuming that this speed is constant in time interval A, the width of this region is estimated to be about 10,000 km to 30,000 km. This calculation assumes that the particle features have a stationary structure and are moving without deformation.

High-time resolution wave data from ISEE 1 are shown in Figure 6. The earliest indication that the broadband electrostatic noise is enhanced occurred at around 1158:30 UT (note that precise timing depends on the frequency channel selected). The enhanced activity is detected from 5.6 Hz to ~31.1 kHz and lasts until about 1205:30 UT. Note the data gaps at 1202 UT and 1210:05 UT. A short burst of electromagnetic noise was observed in the frequency channels 56.2 Hz and 100 Hz at 1159 UT. Another short burst occurred around 1200:30 UT in the frequency channels 100 Hz to 562 Hz. The largest magnetic amplitudes were detected between 1201:30 UT and 1205 UT, mainly in channels below 100 Hz. Note that the enhanced magnetic noise activity was detected much later than the electrostatic activity. The intense magnetic noise activity occurred during intervals B and C and thus coincides closely with the time when the magnetic field became more dipolelike (smaller B_x).

Figure 7 shows another way to present the wave data. Certain wave features are much more clearly identified in data presented in the spectrogram format. The wave data here come from the relaxation sounder experiment which is basically a swept frequency analyzer [*Harvey et al.*, 1978]. At the time the data were taken, this instrument was operating in a passive mode and the sounder was connected to the Mozer antenna system [*Mozer et al.*, 1978]. The sounder was sweeping from 0 Hz to 50 kHz in 128 steps with each step comprising 400 Hz. The duration of each step is 125 ms, and a complete sweep takes 16 s.

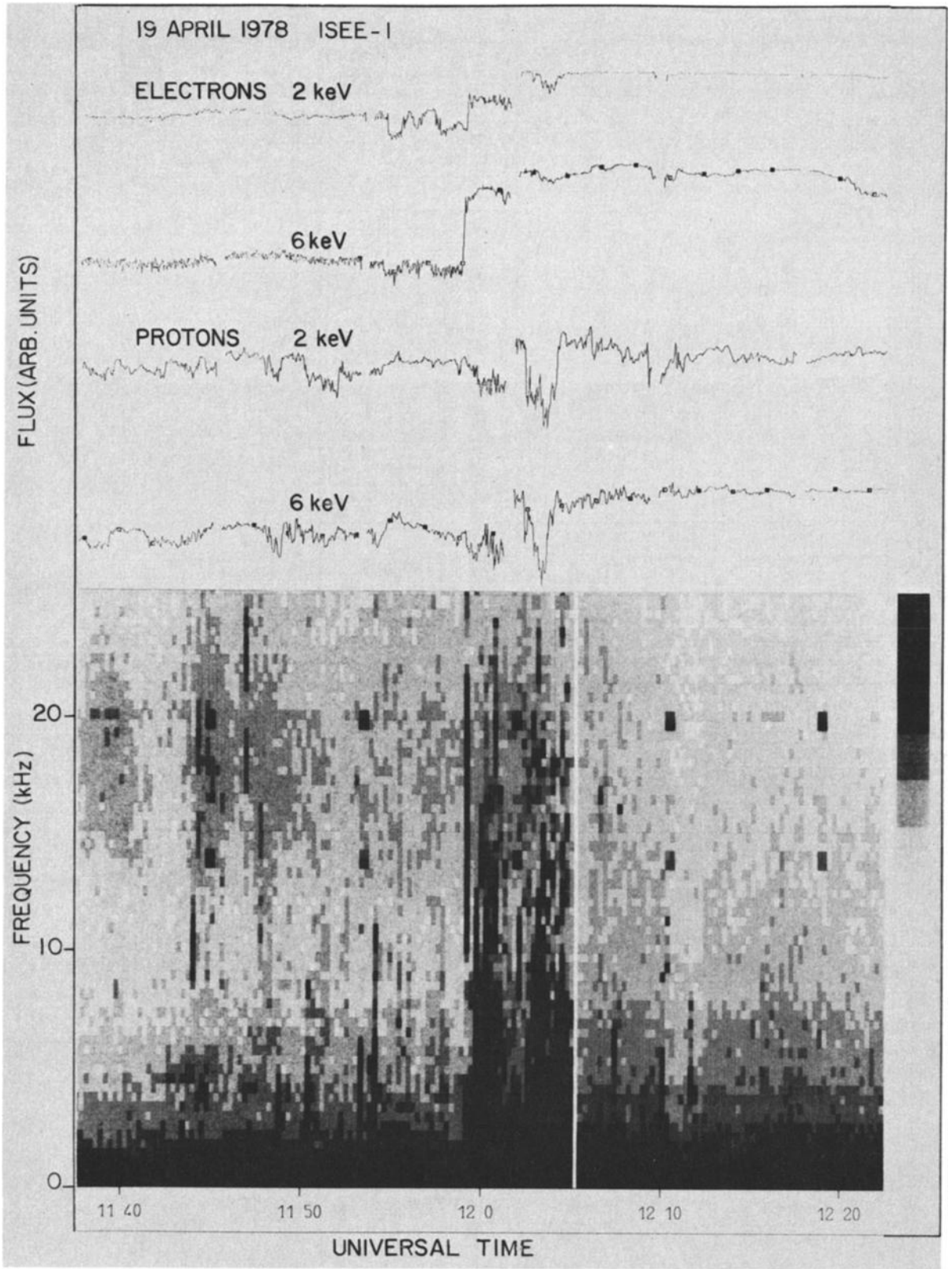

Fig. 7. Electrostatic wave data in the spectrogram format for the 1200 UT event. Darker shade here represents higher wave amplitudes. The enhanced electrostatic waves are observed during the time interval when ion fluxes are low. These waves are confined to a region adjacent to the plasma sheet boundary. Waves are excited to beyond the electron plama frequency.

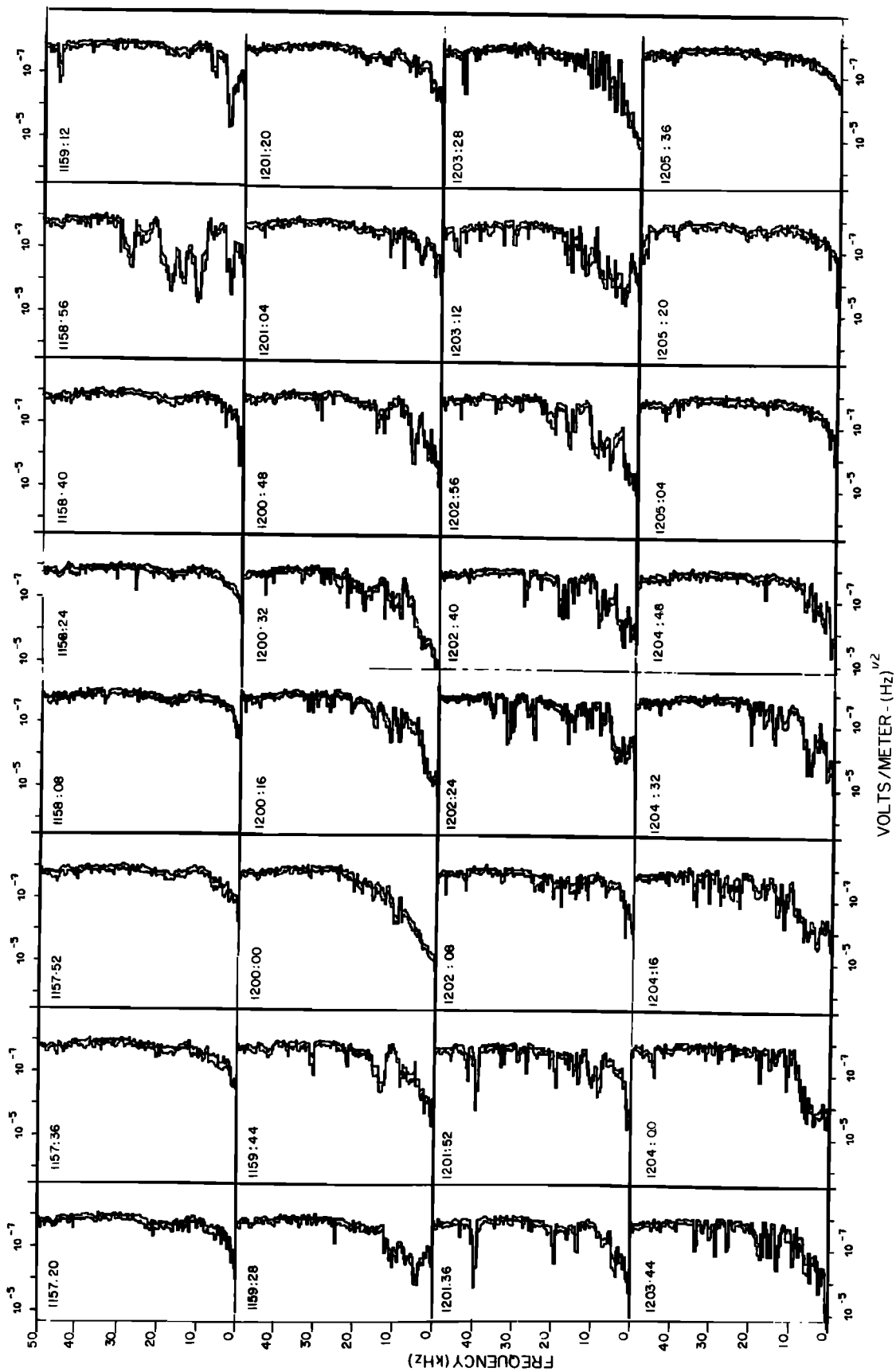

Fig. 8. Frequency spectra of electrostatic waves obtained every 16 s. The spectra are complex with peaks occurring in narrow bands and distributed over a broad frequency interval.

The electrostatic wave activity is enhanced to frequencies greater than 20 kHz (data shown to 25 kHz). The electron plasma frequency determined from the sounder and the propagation experiment (active mode transmits a radio frequency pulse) at 1201 UT is estimated at around 6–8 kHz, and the electron gyrofrequency is estimated at around 1 kHz. Our observations indicate that the electrostatic waves were detected to beyond the electron plasma frequency and the electromagnetic waves to below the gyrofrequency (see Figures 3 and 6). Note the excellent correlation between the wave and the particle data. The enhanced wave activity is confined to the region adjacent to the plasma sheet boundary (intervals A and C) and reduced inside the plasma sheet (intervals B and D). This excellent type of correlation has been observed in more than 10 other events (not shown).

To characterize the behavior of these electrostatic waves further, we show in Figure 8 individual frequency spectra of the waves taken every 16 s [*Harvey et al.*, 1978]. The start time of each sweep is indicated in the upper left corner. The frequency scale (vertical) is linear and the amplitude of the wave (abscissa) is given in V m^{-1} $Hz^{-1/2}$ (recall that the filter frequency is 400 Hz. Thus, the amplitude of the field has been divided by $(400)^{1/2}$). The two lines represent the average amplitude (averaged over 7 samples) and the peak value. Contrast the spectra obtained during the active period (1158:26–1205:20 UT) to those observed at quieter times. Activity is seen to increase over a broad frequency interval from nearly zero to higher than 40 kHz. Note, however, that the activity is distributed in a complicated way. On several occasions (for example, see the spectrum at the onset at 1158:56 UT), the activity was enhanced over a broad frequency range but peaks appear at discrete frequencies (limited bandwidth).

2.4. *Electron Pitch Angle Distributions*

Figures 9*a* and 9*b* show two-dimensional distributions (in GSE system) of electron count rates plotted as a function of the azimuthal angle in GSE reference frame. Distributions from four representative energies are shown in Figure 9*a*. Data here come from the equatorial detector of the experiment flown by *Frank et al.* [1978]. There are sixteen azimuthal sectors in each distribution. The numbers shown on the concentric circles represent the count levels per 1/4-s accumulation period. High count rate in any given sector indicate that the electron fluxes are arriving from that direction. For instance, at 1159:48 UT, 0.102-keV electrons were coming from the earthward direction. The start time of each distribution is shown in the upper left corner together with the energy information. The format of Figure 9*b* is the same as in Figure 9*a* except that each distribution is obtained every spin period (this means that accumulation time per sector is about 3/16 s). Data of Figure 9*b* are derived from the equatorial detector of the experiment flown by *Williams et al.* [1978], and we show only the counts from the 24–34.2 keV (center energy ~ 26.5 keV) channel. When statistically significant count rate is observed in higher energy channels, the behavior is essentially the same as the 26.5-keV electrons (not shown). The direction of magnetic field projected on the ecliptic plane is deduced from the onboard magnetometer. The azimuthal distributions shown here become two-dimensional electron pitch-angle distributions when $B_z = 0$. During our observations, B_z was usually less than 10 nT in a total field of about 50 nT.

Prior to the boundary crossing, 0.102-keV electrons were isotropic, whereas more fluxes were observed at larger pitch angles for the 1.05-keV electrons. No fluxes of electrons were detected above 1.05 keV by the LEPEDEA. Shortly after the boundary crossing at 1159:48 UT, the entire hemisphere facing the earth was lit with 0.102 keV electron fluxes (note that because various energies are stepped sequentially in time, the boundary crossing at 1159 UT was missed). The higher energy electron fluxes (for example, 10.8 keV) had more counts at smaller pitch angles ("field-aligned") and the distributions were bi-directional.

The electron distributions evolve with time and/or space. Beginning around 1202:27 UT, the 1.05 keV and the 5.55-keV electrons are isotropic, and this isotropy is observed to beyond 1207 UT. The 0.102-keV and 10.8 keV electrons become isotropic around 1206 UT. The 26.5-keV electrons are anisotropic from onset to about 1201:54 UT, isotropic until about 1203:07 UT, anisotropic at 1203:46 UT, and isotropic beyond. If we compare the times during which these two types of electron distributions are detected to the times indicated in Figure 4, the picture obtained is that anisotropic (field-aligned) distributions are detected in time intervals A and C and isotropic distributions in time intervals B and D. This feature is most clearly demonstrated in the 26.5 keV electron data.

2.4.1. *Ion pitch angle distributions.* The behavior of ion distributions is shown in Figures 10*a* and 10*b*. The ion count rate in the energy range a few hundred electron volts to several keV was quite low, and the distributions shown in Figure 10*a* come from energy steps where significant counts were detected. Here, before 1159 UT, low counts were detected from the earthward direction. Just after the boundary crossing (1159 UT), particles with large pitch-angles are detected in the dusk quadrant. There is thus a density gradient of these energy particles. These ions are drifting from dusk to dawn as shown in Figure 2. Note the reversal of the density gradient at 1206:48 UT, which is also observed in the flow (see Figure 2).

The higher energy ions at the average energy of 29.1 keV behaved differently from the lower energy ions (Figure 10*b*). Immediately following the onset, these ions were travelling toward the earth. Subsequently, the distributions had significant counts at larger pitch angles. The three distributions on the top right hand column show particles travelling toward the earth. These distributions were observed in time interval C (Figure 4). The last two distributions (bottom two of the right column) are anisotropic, field-aligned and bi-directional, and these were observed in time interval D.

To summarize, in interval A, large density gradient and strong streaming in the earthward direction are observed. In interval B, the particles behaved in a complex way, very differently from those in A. In C we observed behavior much like that in B, but there was also a strong streaming component toward the earth. The behavior in D was similar to B.

2.4.2. *Differential electron energy spectra.* To obtain an overview of the behavior of electrons at different energies, differential electron energy spectra from about 0.1 keV to 270 keV have been constructed from spin averaged data and are shown in Figures 11*a* and 12*a*. If we assume that the spectra observed before the boundary crossing can be fitted by a power law form, the index is about −3 for energies above about 500 eV. (One must exercise caution here in interpreting spin-averaged energy spectral data of complex anisotropic distributions since more than one source could be involved.) The form of the spectra following the boundary crossing is more complicated as there are several spectral components. An interesting feature is the presence of a peak in the energy spec-

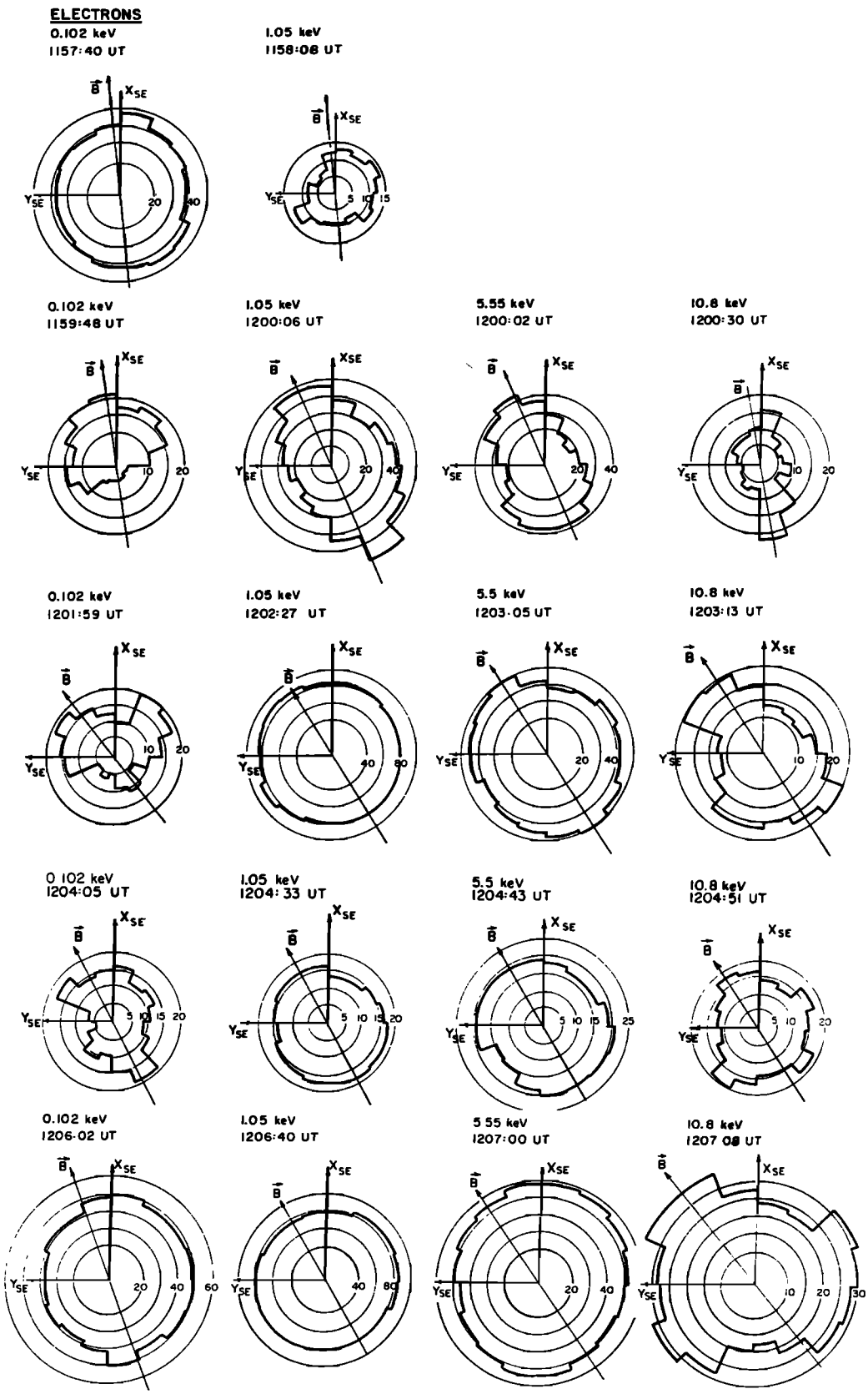

Fig. 9*a*

Fig. 9. (*a*, *b*) Azimuthal distributions of electrons at several energies. The distributions are "field aligned" in the region next to the plamsa sheet boundary and isotropic in the plasma sheet.

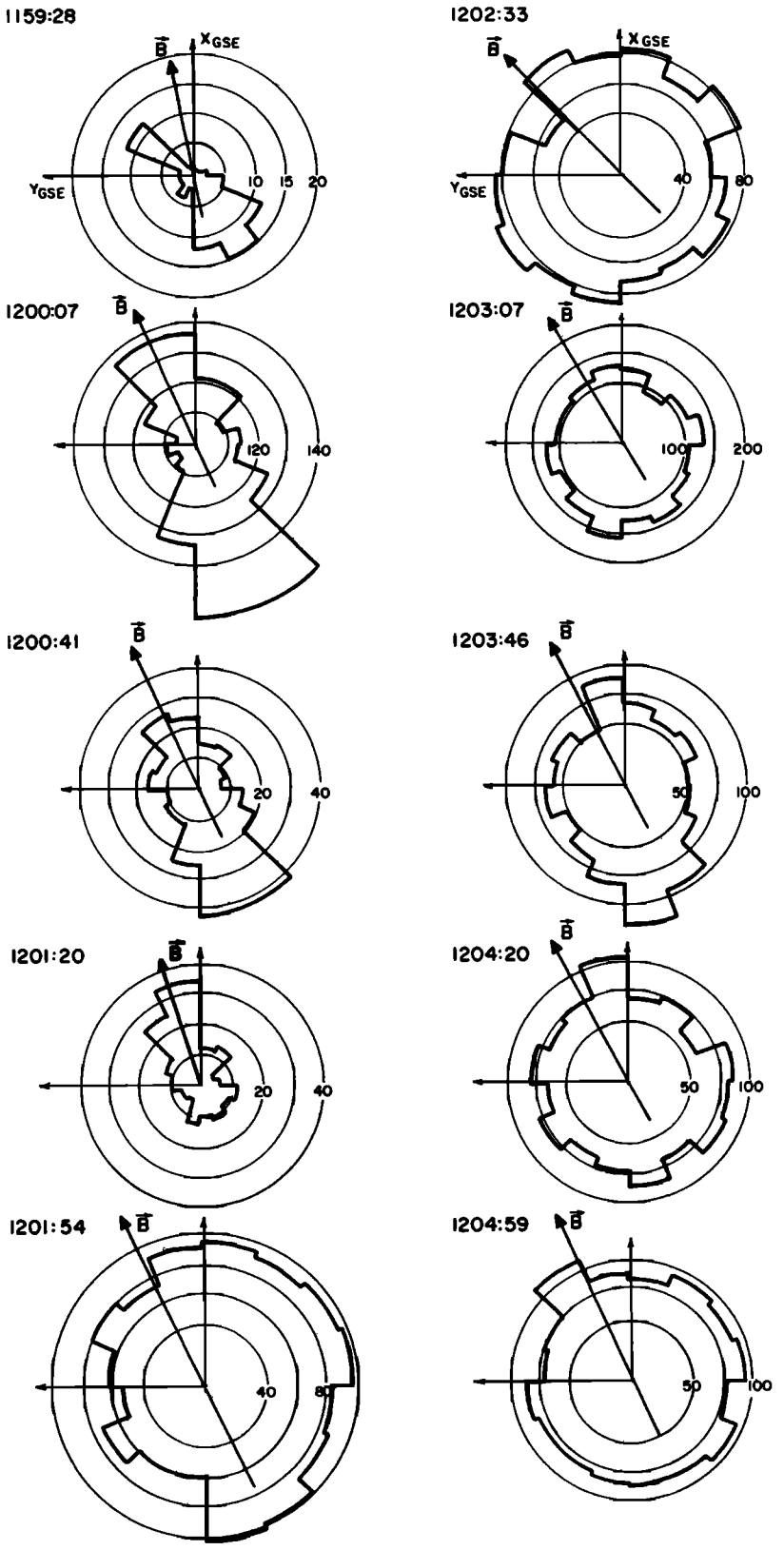
ELECTRONS 26.5 keV
1159:28
1202:33
1200:07
1203:07
1200:41
1203:46
1201:20
1204:20
1201:54
1204:59
B
XGSE
YGSE
10
15
20
40
80
120
140
100
200
20
40
50
100
20
40
50
100
40
80
50
100

Fig. 9*b*

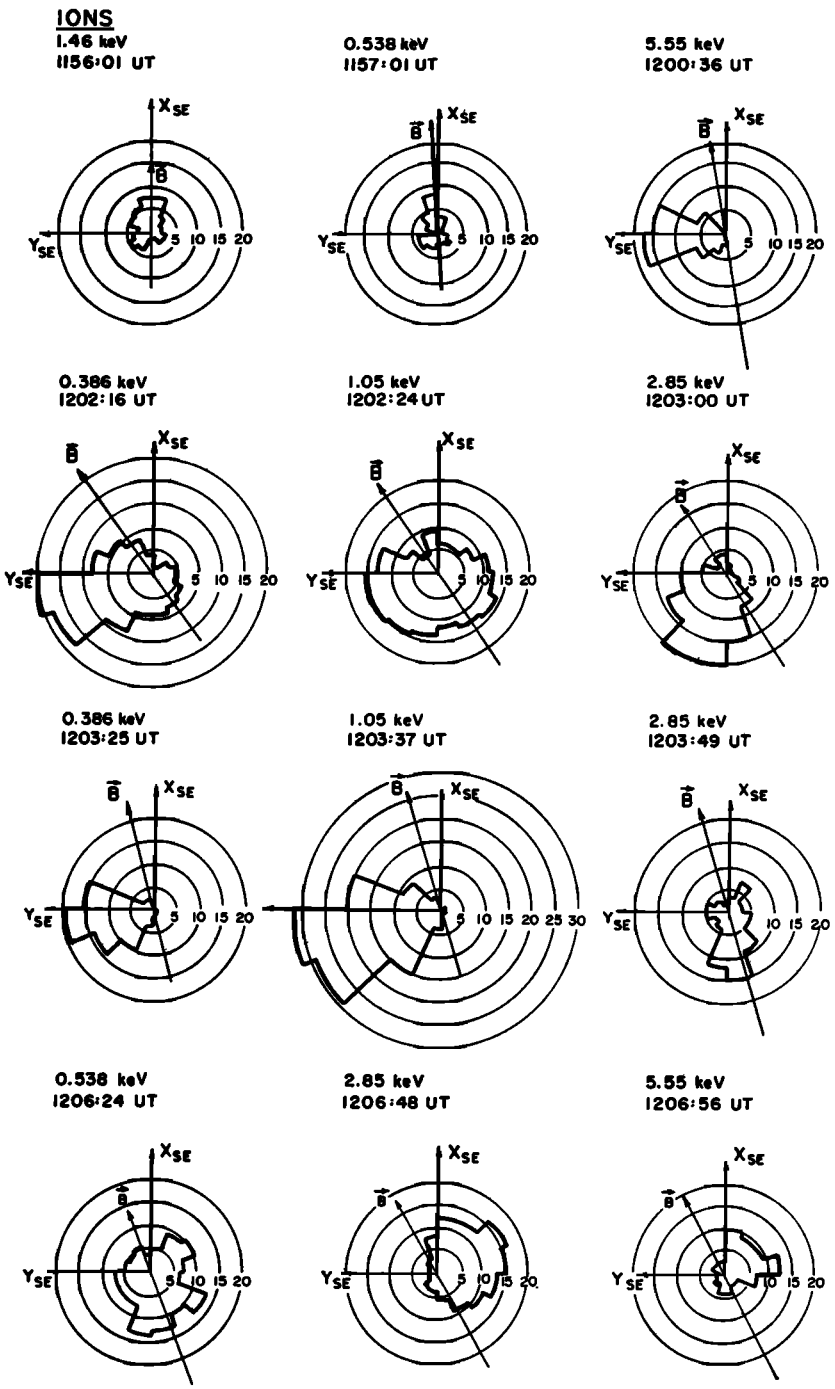

Fig. 10*a*

Fig. 10. (*a*, *b*) Azimuthal distributions of ions at several energies. The behavior of ions is different from the electrons. The low energy ions are convecting perpendicular to **B**. The high-energy ions are field-aligned and travelling toward the earth in the region outside the plasma sheet boundary. Across the plasma sheet boundary, the ions are bi-directional.

trum constructed in the interval 1201 UT–1203 UT (Figure 11*a*). This peak, around 100–300 eV, is still present in the spectrum constructed between 1203 UT and 1205 UT. (The distribution of electrons below 2 keV will be examined in detail below in section 2.4.4.) A small but significant peak was also observed at 60- to 70-keV energies (Figure 12*a*). This peak is not present in the spectrum constructed at 1202:38 UT. The peaks in spectra were detected in the time interval A through C (Figure 4).

Complex energy spectra can be approximated by either a superposition of two or more power law forms or portions by a Maxwellian. For instance, for the spectrum constructed between 1203–1205 UT, the index is around -1.4 in the energy interval a few hundred electron volts to several keV, and about -3 for energies above about 10 keV. This index also describes electrons of higher energies (Figure 12*a*). The complex behavior of electron energy spectra in the geomagnetic tail has been observed since 1966 [*Konradi*, 1966]. A simple

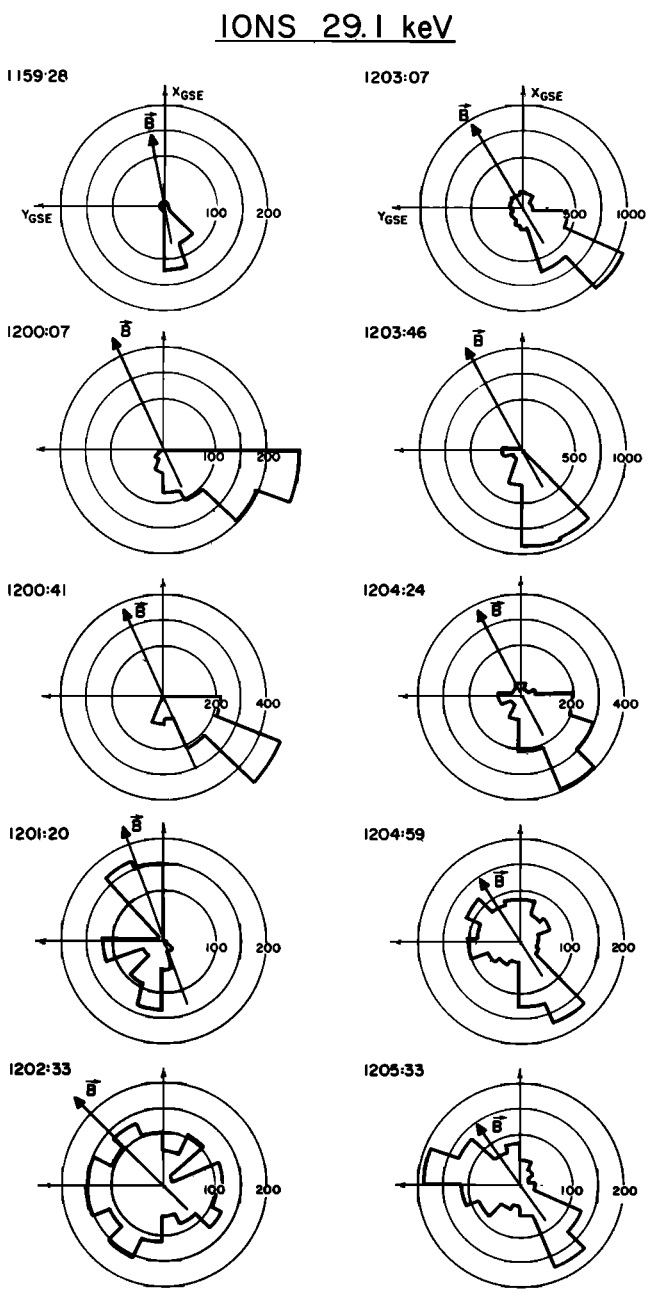

Fig. 10*b*

interpretation of the complex spectral forms is that there is more than one source of electrons.

2.4.3. *Differential ion energy spectra.* The general behavior of differential ion energy spectra constructed from spin-averaged ion fluxes are shown in Figures 11*b* and 12*b*. The ions in the interval 1155–1209 UT were composed of ~91% H^+, 5% O^+, and 4% He^{++} (W. Lennartsson, private communication, 1984). The spectra before the boundary crossing for energies greater than several keV can be described by a power law form with an index of about −3. Recall that this was the same index for the electrons. Like the electrons, the spectral forms subsequent to the onset are much more complicated, and there are several spectral components present with peaks observed at various energies.

The variability of ion spectra has been observed since the first observations of ions in the geomagnetic tail [*Konradi*, 1966]. More recent observations [*Williams*, 1981] have related the energy spectral characteristics of ions to the dynamics of the geomagnetic tail. *Williams* [1981] has further shown that many of the spectral features can be understood in terms of single particle dynamics in which the first particle invariant is conserved.

We will end this section by noting that the ion spectra appear to be in some way more dynamic than the electron spectra. The low-energy portion (energies below a few keV) represents ions that are often dominated by convection (Figure 2). The high energy portion represents ions that are anisotropic, some streaming toward the earth, and others bi-directional. Peaks in energy spectra are associated with these streaming particles.

2.4.4. *Electron distributions below 2 keV.* Electron distributions below 2.062 keV from the experiment of *Ogilvie et al.* [1978] will now be studied to learn more about the behavior of the low energy particles. Two-dimensional distribution contours $f(v_{||}, v_\perp)$ in the phase space defined by $(v_{||}, v_\perp)$ and reduced distributions $F(v_{||}) = 2\pi\int v_\perp f(v_{||}, v_\perp)dv_\perp$ are shown in Figures 13*a* through 13*p*. These distributions are transformed to the coordinate frame moving with the electron bulk velocity travelling antiparallel to the direction of the geomagnetic field. It takes 3 s to construct each set of distributions, and this is done sequentially at 9-s intervals. The start times of each distribution are shown on the upper left corner. The abscissa is $v_{||}$ and the ordinate of the contour plots is $v_\perp$. The ordinate of $F(v_{||})$ is the value of the reduced distribution in units of s cm^{-4}, and the integral of $F(v_{||})$ gives the total number density of electrons travelling parallel and antiparallel to the direction of the magnetic field. The velocity scales are 0 to 30×10^8 cm/s for $v_\perp$ while for $v_{||}$ the values are from -30×10^8 to $+30 \times 10^8$ cm/s. Here, the minus sign denotes electrons travelling against the direction of the magnetic field. The magnetic field is directed to the right as shown. Thus, the positive sign denotes electrons travelling along the direction of the field (earthward) and the minus sign denotes electrons travelling against the magnetic field (tailward). There are three sets of distributions per row, each row designated by letters "a" through "p".

A circular distribution contour represents electrons with symmetric and isotropic distribution function. At approximately 1159:07 UT (row "b", middle distributions), the distribution contours abruptly depart from the circular shape. Here, $f_{||}$ is larger than $f_\perp$ indicating the distribution is more field aligned. At the same time, we see from the reduced distribution function a small plateau for earthward-going electrons and a small bump for tailward going particles. This is a classic "bump on tail" reduced distribution. The anisotropic distribution contours are observed until about 1202 UT (row "h"). The contours during the interval 1202:09 UT and 1202:45 UT are isotropic, and the reduced distributions fairly smooth (rows "i" and "j"). The distribution function is once more anisotropic and lasts until about 1204:44 UT (or a little later). After this, the distribution function is again isotropic (rows "o" and "p").

Comparison of the times when the two types of distribution function are observed to the times in Figure 4 will indicate that anisotropic distribution functions were observed in time intervals A and C. Distribution functions in intervals B and D were isotropic. During time intervals A and C, the reduced distributions are structured with plateaux and bumps having positive slopes, $\partial F/\partial v_{||} > 0$. On the basis of a propagation of error analysis [*Fitzenreiter et al.*, 1984], which determines the

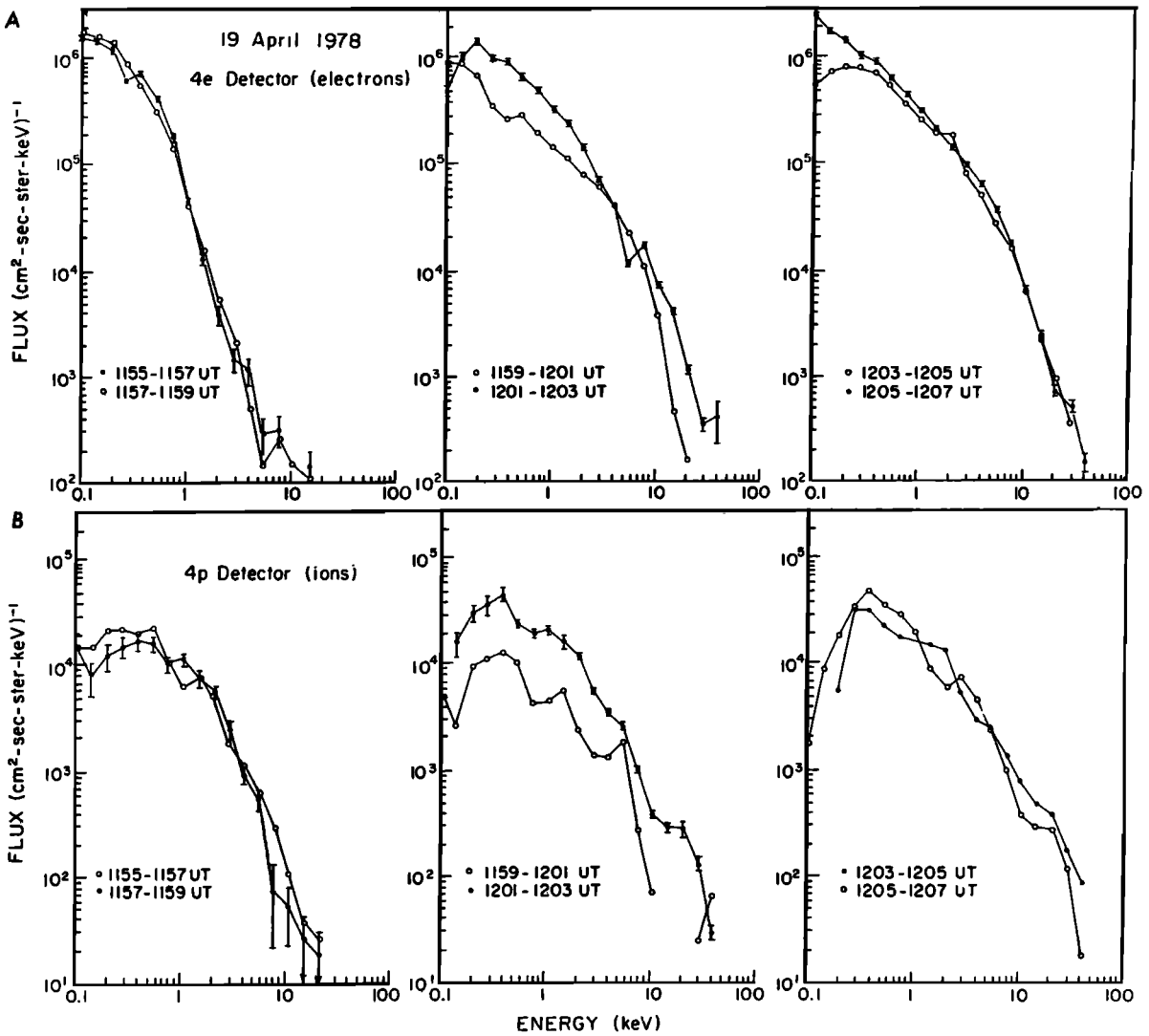

Fig. 11. (*a*) Differential electron energy spectra sampled at different times from LEPEDEA. Note the peaks around 100–400 eV. (*b*) Ion differential energy spectra sampled at several time intervals.

effect of statistical fluctuations in electron counts on the reduced distribution, the positive slope structures corresponding to tailward going beams seen at times 1159:07 UT, 1200:20 UT, and 1201:50 UT are better than 68% significant.

Another way to display the reduced distribution function data is to plot them as a function of time. Figure 14 shows these plots for electrons travelling parallel and antiparallel to **B** for the various energies indicated. The behavior in the two directions is essentially the same. In both plots the reduced distribution functions show a strong energy dependence. Between 1159 UT and 1202 UT, the sharp increase observed at around 641 eV was accompanied by a decrease for energies less than about 200 eV (note that this feature could also be seen in Figure 11*a*). The reduced distributions in the energy interval about 200 eV to 600 eV were nearly constant. Data here indicate that the energy structure of the region adjacent to the plasma sheet boundary was characterized on April 19, 1978 by a decrease in the phase density of low energy parallel electrons (less than about 200 eV), an increase in phase space density above about 600 eV, and nearly constant at intermediate energies (200–600 eV).

Information on the net fluxes of electrons traveling in the two directions of the magnetic field can be obtained. Figure 15 shows this as a function of the universal time. The net fluxes were computed by taking the difference of particles travelling in the two directions. In the time interval 1159 UT and 1202 UT (interval A), the net flux was negative, meaning more fluxes were detected from the earthward direction. In time intervals B, C, and D, more fluxes are detected toward the earth. Note, however, that there is a considerable amount of fluctuation in the data.

The fact that there are measurable net fluxes suggests that there are field-aligned currents in these regions. In the region adjacent to the plasma sheet boundary (see Figure 4 for comparison), the current was directed toward the earth (interval A). The current was directed toward the tail inside the plasma sheet (time intervals B and D). (The exact relationship between these currents and changes in B_y is complex and will not be discussed here.) An estimate of field-aligned current intensity for the 1159–1202 UT interval when significant peaks were observed in the reduced distributions has been made (interval A). If we use $nv_{\parallel}$ as about 5–10 $\times$ 10^6 $(cm^2\ s)^{-1}$, a current of about 10^{-8} to 2 $\times$ 10^{-8} A/m^2 is obtained. This value is comparable to the value reported by *Frank et al.* [1981] for the

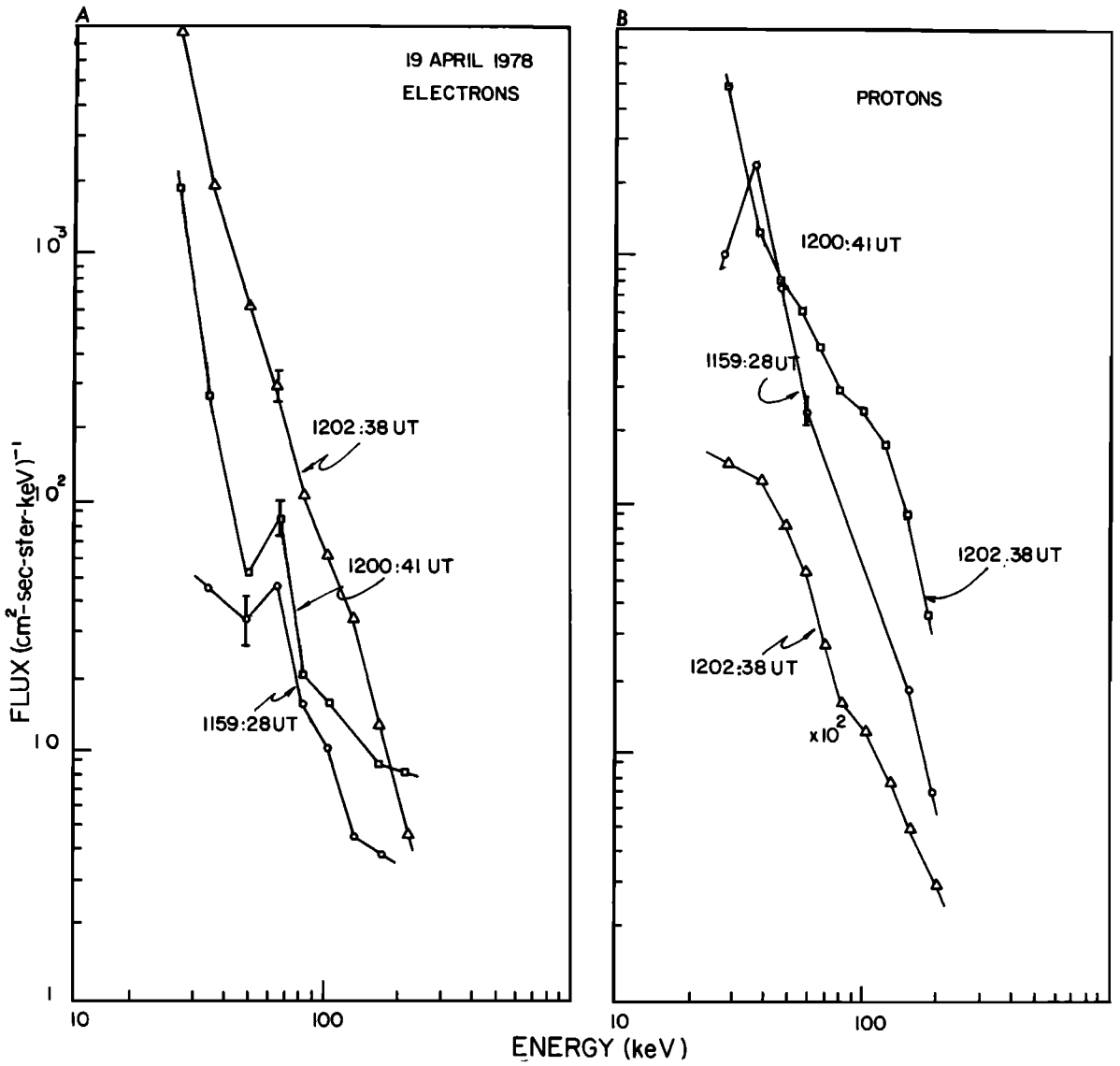

Fig. 12. (*a*) Differential electron energy spectra sampled at different times from the medium energy experiment. Note the peaks around 60–90 keV. (*b*) Ion differential energy spectra sampled at several time intervals.

tail event of March 26, 1978. These net fluxes were measured from a few electron volts to about 2-keV electrons.

3. Summary and Discussion

The existence of a narrow region immediately adjacent to the high-latitude boundary of the plasma sheet was first identified in the ISEE particle data for events encountered on March 2, 1978 [*Parks et al.*, 1979]. We have since examined over several hundred plasma sheet particle events encountered in the geomagnetic tail in 1978 and 1979, and the picture that emerges is that this region is a persistent feature of the plasma sheet boundary. Observations of this region under diverse geomagnetic conditions show that the spatial dimension can be as small as 100 km (which is roughly the gyroradius of one keV ions) or can extend to more than ten thousand kilometers (not shown). The structure is also strongly dependent on the energy and species of the particles. In the example shown in this paper, which is fairly typical, the region was characterized by an increase of a few keV electrons, while ions with energies less than about 6 keV decreased (Figure 4). The phase space density of electrons below about 2 keV showed that for electrons travelling along and against the direction of the geomagnetic field, a decrease was observed at energies below about 200 eV, a constant value between 200 and 600 eV, and an increase above 600 eV (Figure 15). This region also frequently supports a field-aligned current. For the April 19, 1978, event, the presence of a field-aligned current was inferred from the net fluxes of less than 2-keV electron fluxes travelling along and against the direction of the magnetic field and as well from the signatures of the magnetic B_y component.

Our examination of particle data from several experiments indicates that the behavior of the distribution functions in this narrow region is distinctly different from that observed in the lobe and deeper in the central plasma sheet. Electrons over a broad energy interval are "field-aligned" and bi-directional, whereas in the plasma sheet the distributions are more isotropic. For the event we studied, low-energy ions (below a few keV) were being convected, and the most intense flows are primarily confined to the narrow region of the plasma sheet boundary layer. These intense ion flows do not appear to be

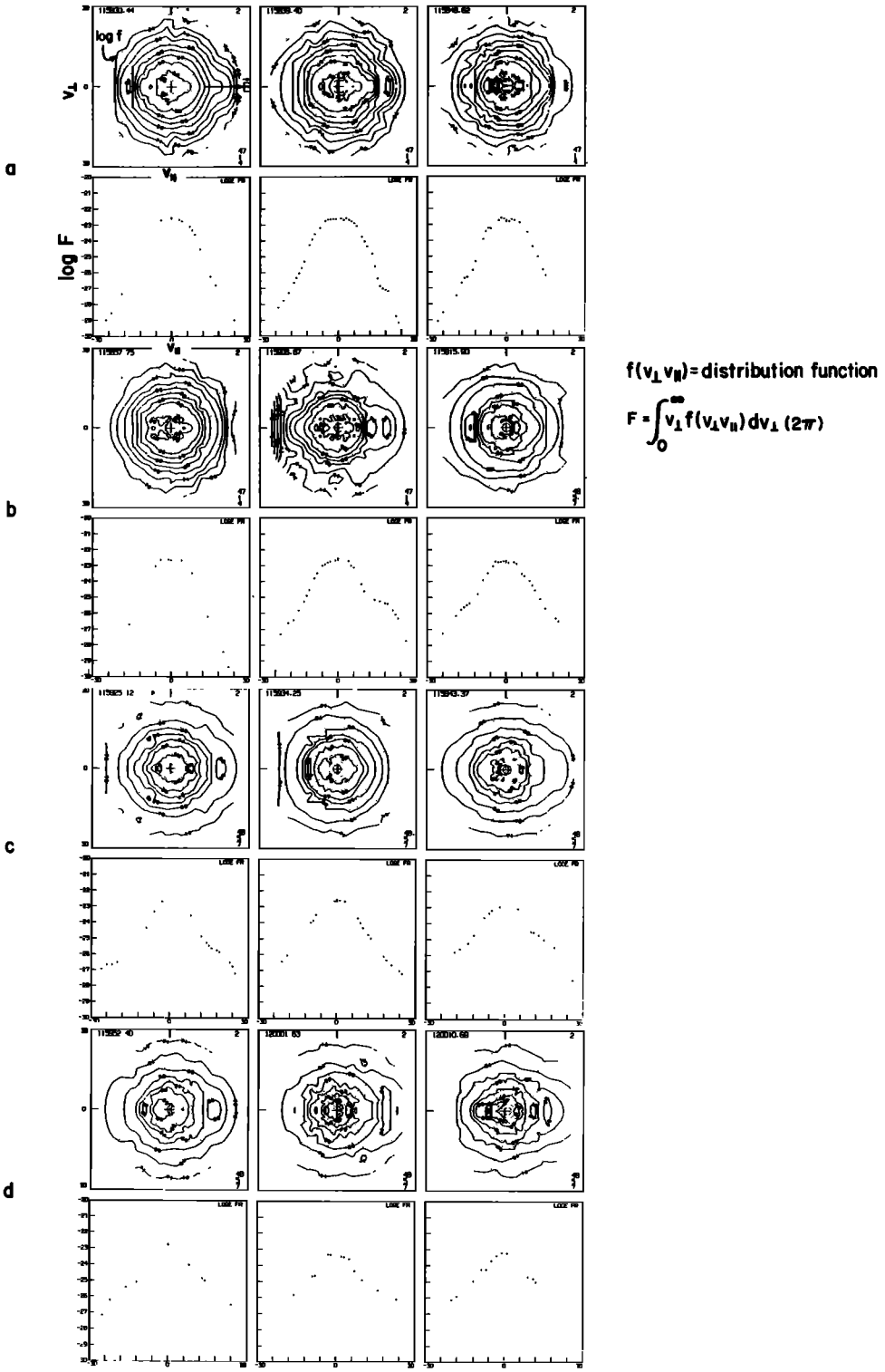

Fig. 13. (*a–p*) Plots of distribution function in the velocity space and reduced distribution plotted against $v_{||}$. There are three sets of these distributions per row, marked *a* through *p*. It takes 3 s to construct a set, and the successive distributions are separated by 9 s. The distributions in the region where the waves are confined are anisotropic. Also, note peaks and plateaus in the reduced distributions.

organized in any systematic way, as flows are observed in all directions, and they change directions rapidly and frequently. This erratic flow behavior is consistent with the behavior of large-amplitude electric fields that are observed in the region. The high-energy ions (above ~10 keV) are also field-aligned and propagating toward the earth, whereas the distributions in the plasma sheet are field-aligned and bi-directional. A persistent feature of low-energy electron distributions (<2 keV) is that they are generally anisotropic with $f_{||}$ larger than $f_\perp$, whereas they are nearly isotropic in the plasma sheet. The

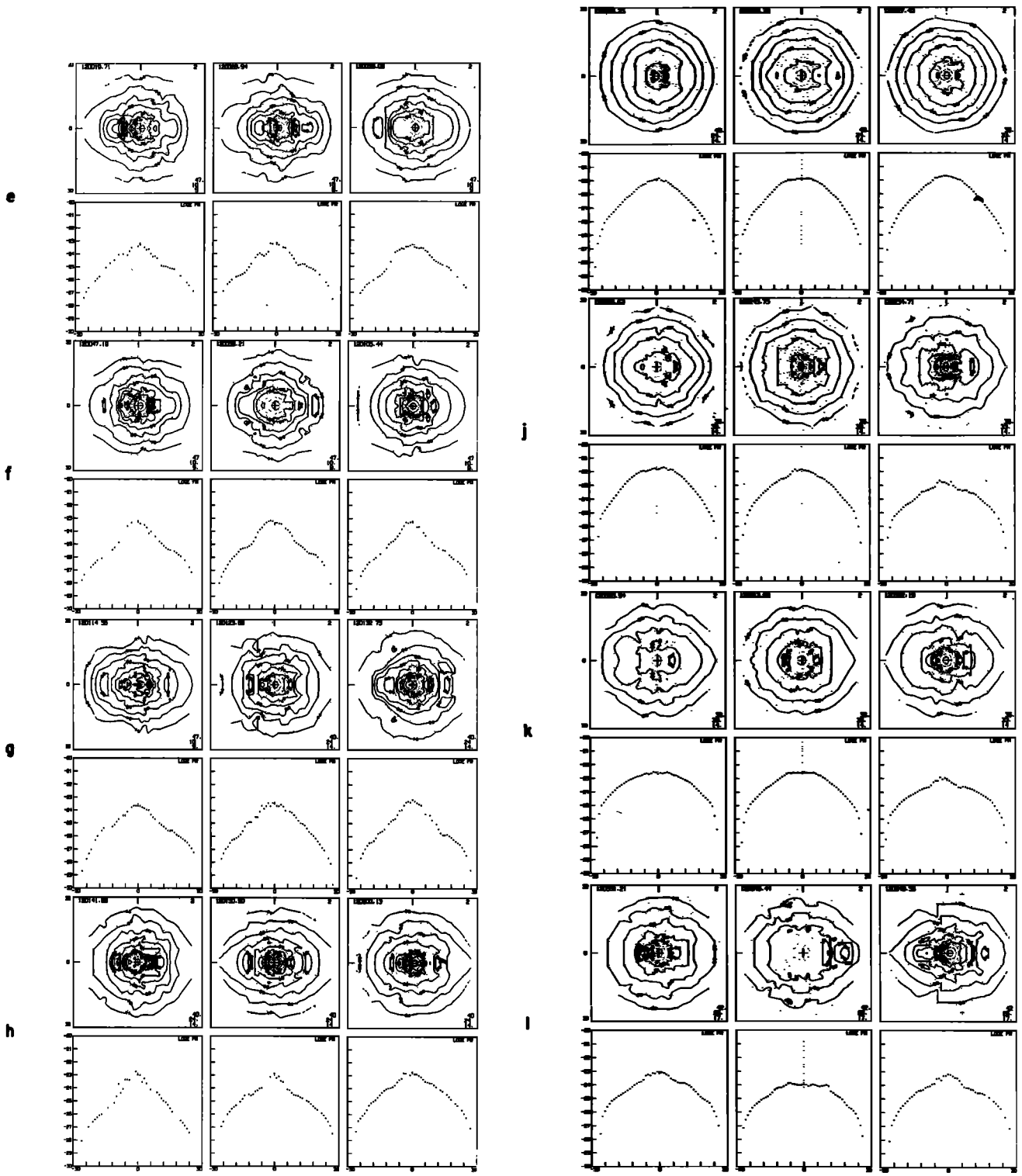

Fig. 13 (continued)

reduced distributions show prominent peaks and plateaus that indicate that the plasma distributions there include a beam component. This observation means that the distribution function in the phase space has a positive slope, $\partial F(v_{\|})/\partial v_{\|} > 0$, which is quite unstable to a variety of electrostatic instabilities. The beam is sometimes fairly intense. During 1159 UT to 1202 UT on April 19, 1978, the net flux from the earthward direction was about 5×10^6 to 10^7 $(\text{cm}^2\ \text{s})^{-1}$. These electrons have a velocity of about 10^9 cm/s. The beam density is thus estimated to be as large as about 10^{-3} to 10^{-2} cm^{-3}. Because the ambient plasma density during this time interval was about 0.5 cm^{-3}, the beam to ambient density ratio n_b/n_p is about 5×10^{-3} to 5×10^{-2}. Thus, the beam can comprise a sufficient fraction of the total plasma density that, when con-

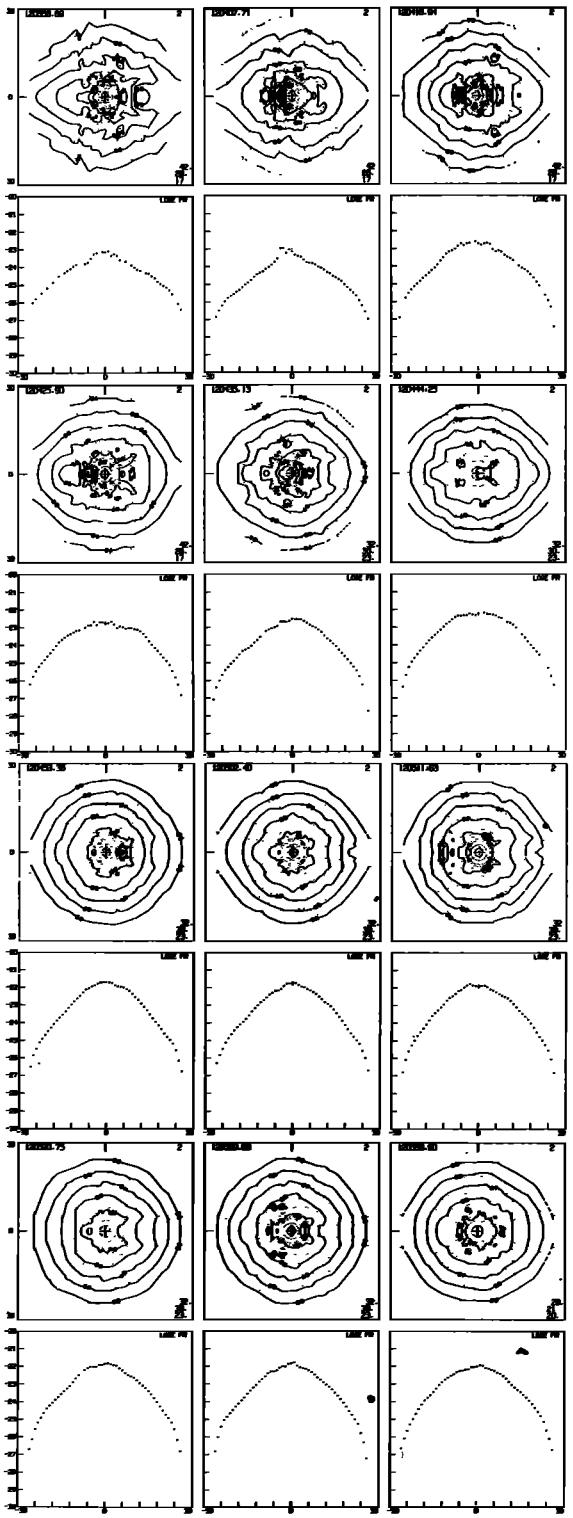

Fig. 13 (continued)

sidering instabilities of the beams, strong beam plasma effects must be considered.

The broadband electrostatic wave activity is enhanced and confined primarily in the narrow region adjacent to the plasma sheet boundary. The frequency spectra of these waves are extremely complex, with activity being observed over a broad frequency interval but with peaks appearing at discrete frequency intervals. The frequency spectra are quite dynamic, and various fairly narrow peaks appear and disappear in successive individual spectra (16-s time resolution). The wave power is mostly enhanced below about 20–30 kHz, and significant enhancement is observed to beyond the local plasma frequency. The amplitude of these waves can reach several millivolts per meter.

Broadband electrostatic noise is also observed at ionospheric heights [*Gurnett and Frank*, 1977]. These ionospheric waves are observed in a narrow region poleward of >45 keV trapping boundary. The region in which these waves are confined is populated with enhanced fluxes of 100 eV–1 keV energy electrons. These features are quite reminiscent of plasma characteristics observed in the geomagnetic tail where similar electrostatic noise is observed. These two regions may be interconnected. We showed that the electrons in the beams were observed coming from the earthward direction. Assuming that these electrons are accelerated at auroral ionospheric heights, it is then very possible that these beam electrons could contribute significantly to the generation of electrostatic waves in both regions of space. If indeed this picture is correct, then the region adjacent to the high-latitude boundary of the plasma sheet is conjugate to a region poleward of the >45 keV trapping boundary at auroral ionospheric heights.

The current theoretical understanding of the electrostatic wave generation mechanisms [*Huba*, 1978; *Swift*, 1981; *Grabbe and Eastman*, 1984] is based on the correlation studies made between waves and ions [*Gurnett et al.*, 1976]. Instabilities considered in these papers include waves excited by ion flows and lower hybrid drift waves. The frequency of the waves here is generally below the local electron plasma frequency, and consequently, these mechanisms, while they contribute to the waves observed below a few kHz in the geomagnetic tail, they cannot explain the waves observed at higher frequencies. Another possible mechanism for electrostatic waves below the electron plasma frequency is due to $f_{||} > f_{\perp}$. In such a case, electrostatic electron cyclotron waves become unstable [*Young et al.*, 1973]. However, the conditions of this instability require the presence of cold plasma, and the frequency spectra tend to be quite narrow. Since the frequency spectra shown are 16-s spectra, it is possible that the observed spectra represent the superposition of many narrow peaks. If this does occur, the instability studied by *Young et al.* [1973], which was used to explain substorm associated electrostatic waves observed closer to earth, cannot be ignored.

If the electron beams were responsible for the enhanced electrostatic waves, especially for the high-frequency waves (waves above the local electron plasma frequencies), we should in principle expect the beam to diminish as the wave energy is increased. However, this simple picture is not revealed in the data. A part of the complexity arises because an enhanced wave spectrum often consists of several peaks and it is not immediately obvious which of the peaks is directly related to the beam. Then there is the question of why there are several spectral peaks. Are these different peaks due to the fact that the beam energy and/or other beam parameters are changing in time? To what extent are the features due to strong beam-plasma interactions, and are there features due to nonlinear wave–wave interactions? For instance, are the waves below the electron plasma frequency consequences of nonlinear decay of the high-frequency waves, or are they consequences of other instabilities that operate below the electron plasma frequency? What role does the field-aligned current play in these instabilities? These questions are not resolved and require further study.

Finally, it should be noted that the plasma and wave

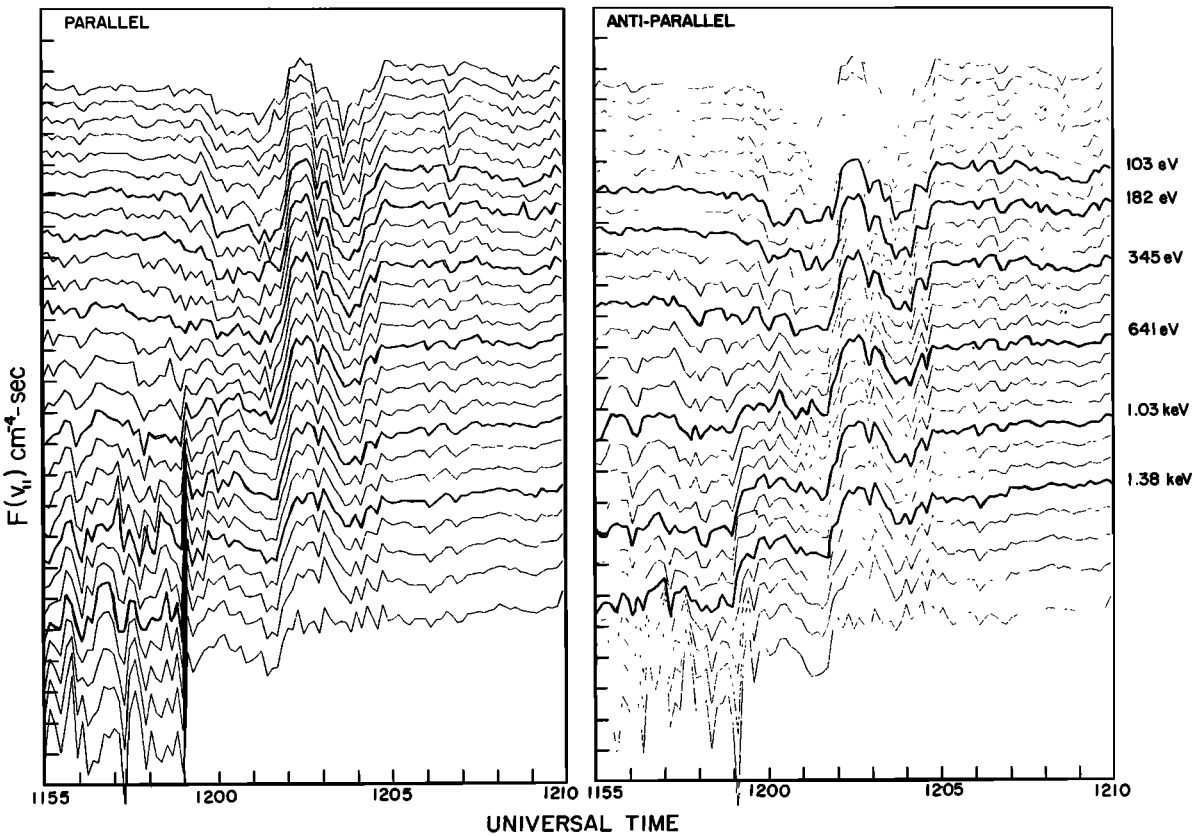

Fig. 14. Reduced distributions are plotted as a function of universal time for electrons travelling parallel (earthward) and antiparallel (tailward) to **B**. The region adjacent to the plasma sheet boundary is characterized by a depletion of electrons below 200 eV, by a constant flux for electrons 200–600 eV, and by an increase of electrons with energies greater than 600 eV.

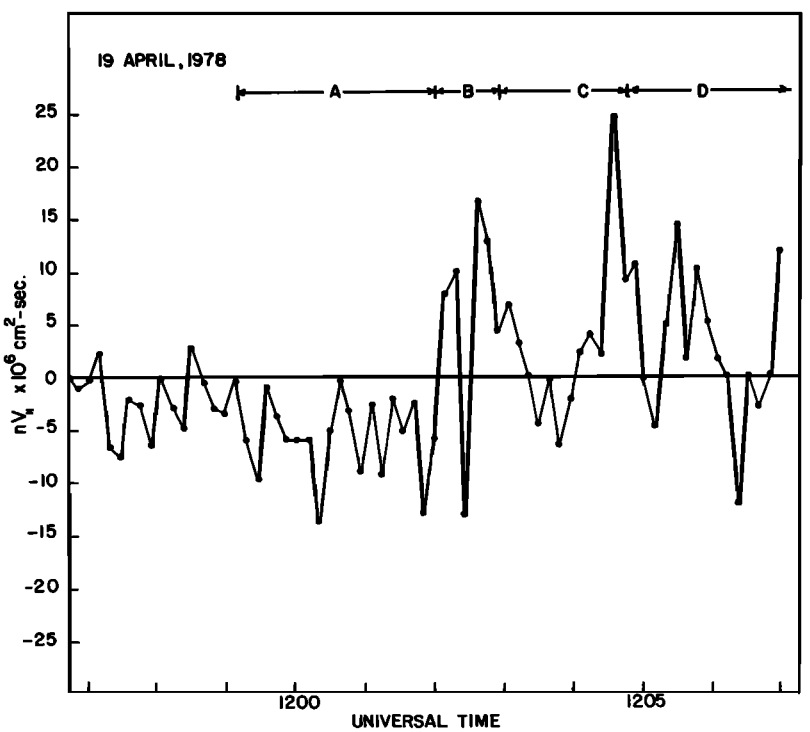

Fig. 15. Net electron fluxes in the direction parallel and antiparallel to **B** plotted as a function of universal time. The net flux in the region adjacent to the plasma sheet boundary is directed toward the tail. In the plasma sheet, the net flux is primarily directed toward the earth.

characteristics observed on ISEE spacecraft are for distances of less than 23 R_E in the geomagnetic tail. However, we know from the observations of *Scarf et al.* [1974] and *Gurnett et al.* [1976] that similar features are to be expected to distances of 35 R_E. Does this region exist at 200 R_E? In this regard, we find it extremely interesting that enhanced broadband electrostatic noise has been observed by ISEE 3 spacecraft in the geomagnetic tail at 230 R_E distances [*Scarf et al.*, 1984]. The characteristics of these waves should be studied in conjunction with the plasma data in order to ascertain whether these waves are also confined adjacent to the plasma sheet boundary and whether electron beams survive to such large distances.

Acknowledgments. We thank the UCLA group for the high-time resolution magnetic field data and W. Lennartsson for giving us information on ion composition. The ISEE project is a joint NASA/ESA program, and we are indebted to both organizations for their efforts that made the program successful. Data analysis support for U.S. programs come from the ISEE project office. The research at the University of Washington is supported in addition by a National Science Foundation grant (ATM-8300164).

The Editor thanks W. Lennartsson and another referee for their assistance in evaluating this paper.

REFERENCES

Aggson, T. L., Observations of large magnetospheric electric fields during the onset phase of a substorm, *J. Geophys. Res.*, *88*, 2981, 1983.

Anderson, K. A., Energetic electron fluxes in the tail of the geomagnetic tail, *J. Geophys. Res.*, *70*, 4741, 1965.

Anderson, K. A., R. P. Lin, R. J. Paoli, G. K. Parks, C. S. Lin, H. Reme, J. S. Bosqued, F. Martel, F. Cotin, and A. Cros, An experiment to study energetic particle fluxes in and beyond the Earth's outer magnetosphere, *IEEE Trans. Geosci.*, *GE-16*, 213, 1978.

Baker, D. N., R. D. Balian, P. R. Higbie, and E. W. Hones, Jr., High-energy magnetospheric protons and their dependence on geomagnetic and interplanetary conditions, *J. Geophys. Res.*, *84*, 7138, 1979.

Cattell, C., M. Kim, R. P. Lin, and F. Mozer, Observations of large electric fields near the plasma sheet boundary by ISEE 1, *Geophys. Res. Lett.*, *9*, 539, 1982.

Cowley, S. W. H., and D. J. Southwood, Some properties of a steady state geomagnetic tail, *Geophys. Res. Lett.*, *7*, 833, 1980.

DeCoster, R. J., and L. A. Frank, Observations pertaining to the dynamics of the plasma sheet, *J. Geophys. Res.*, *84*, 5099, 1979.

Eastman, T. E., L. A. Frank, W. K. Peterson, and W. Lennartsson, The plasma sheet boundary layer, *J. Geophys. Res.*, *89*, 1553, 1984.

Eastman, T. E., L. A. Frank, and C. Y. Huang, The boundary layers as the primary transport regions of the earth's magnetotail, *Rep. 83-7*, Univ. of Iowa, Iowa City, Feb. 1983.

Fairfield, D. H., Magnetic field signatures of substorms on high latitude field lines in the night time magnetotail, *J. Geophys. Res.*, *78*, 1553, 1973.

Fitzenreiter, R. J., A. J. Klimas, and J. D. Scudder, Detection of bump-on-tail reduced electron velocity distributions at the electron foreshock boundary, *Geophys. Res. Lett.*, *11*, 496, 1984.

Frank, L., A survey of electrons $E > 40$ keV beyond 5 earth radii with Explorer 14, *J. Geophys. Res.*, *70*, 1593, 1965.

Frank, L. A., D. M. Yeager, H. D. Owens, K. L. Ackerson, and M. R. English, Quadrispherical LEPEDEAS for ISEE's-1 and -2 plasma measurements, *IEEE Trans. Geosci.*, *GE-16*, 221, 1978.

Frank, L. A., R. L. McPherron, R. J. DeCoster, B. G. Burek, K. A. Ackerson, and C. T. Russell, Field-aligned currents in the earth's magnetotail, *J. Geophys. Res.*, *86*, 687, 1981.

Grabbe, C. L., and T. E. Eastman, Generation of broadband electrostatic noise by ion beam instabilities in the magnetotail, *J. Geophys. Res.*, *89*, 3865, 1984.

Gurnett, D. A., and L. A. Frank, A region of intense plasma wave turbulence on auroral field lines, *J. Geophys. Res.*, *82*, 1031, 1977.

Gurnett, D. A., L. A. Frank, and R. P. Lepping, Plasma waves in the distant magnetotail, *J. Geophys. Res.*, *81*, 6059, 1976.

Gurnett, D. A., F. L. Scarf, R. W. Fredericks, and E. J. Smith, The ISEE-1 and ISEE-2 plasma wave investigation, *IEEE Trans. Geosci.*, *GE-16*, 225, 1978.

Harvey, C. C., J. Etcheto, Y. DeJavel, R. Manning, and M. Petit, The ISEE electron density experiment, *IEEE Trans. Geosci.*, *GE-16*, 231, 1978.

Huba, J. D., N. Gladd, and K. Papadopolous, Lower hybrid drift wave turbulence in the distant magnetotail, *J. Geophys. Res.*, *83*, 5217, 1978.

Ipavich, F. M., and M. Scholer, Thermal and suprathermal protons and alpha particles in the earth's plasma sheet, *J. Geophys. Res.*, *88*, 150, 1983.

Konradi, A., Electron and proton fluxes in the tail of the magnetosphere, *J. Geophys. Res.*, *71*, 2317, 1966.

Lui, A. T. Y., E. W. Hones, Jr., F. Yasuhara, S. I. Akasofu, and J. S. Bame, Magnetic plasma flow during plasma sheet expansions: Vela 5 and 6 and IMP 6 observations, *J. Geophys. Res.*, *82*, 1235, 1977.

Lui, A. T. Y., T. Eastman, D. Williams, and L. Frank, Observations of ion streaming during substorms, *J. Geophys. Res.*, *88*, 7753, 1983.

Mobius, E., F. M. Ipavich, M. Scholer, G. Glockler, D. Hovestadt, and B. Klecker, Observations of a nonthermal ion layer at the plasma sheet boundary during substorm recovery, *J. Geophys. Res.*, *86*, 5143, 1980.

Mozer, F. S., R. B. Torbert, V. Fahleson, G. Falthammar, A. Gonfalone, and A. Pedersen, Measurements of quasi-static and low frequency electric fields with spherical double probes on the ISEE-1 spacecraft, *IEEE Trans. Geosci.*, *GE-16*, 258, 1978.

Ogilvie, K., J. D. Scudder, and H. Doong, The electron spectrometer experiment on ISEE-1, *IEEE Trans. Geosci.*, *GE-16*, 261, 1978.

Parks, G. K., C. S. Lin, K. A. Anderson, R. P. Lin, and H. Reme, ISEE 1/2 observations of outer plasma sheet boundary, *J. Geophys. Res.*, *84*, 6471, 1979.

Pedersen, A., C. Cattell, C. Falthammar, V. Formisano, P. A. Lindqvist, F. Mozer, and R. Torbert, Quasi-static electric field measurements with spherical double probes on GEOS and ISEE satellites, *Space Sci. Rev.*, in press, 1983.

Peterson, W. K., R. D. Sharp, E. G. Shelley, R. G. Johnson, and H. Balsinger, Energetic ion composition of the plasma sheet, *J. Geophys. Res.*, *86*, 761, 1981.

Russell, C., The ISEE 1 and 2 flux gate magnetometer, *IEEE Trans. Geosci.*, *GE-16*, 239, 1978.

Scarf, F. L., L. A. Frank, K. L. Ackerson, and R. P. Lepping, Plasma wave turbulence at distant crossings of the plasma sheet boundaries and the neutral sheet, *Geophys. Res. Lett.*, *1*, 189, 1974.

Scarf, F. L., F. V. Coroniti, C. F. Kennel, R. W. Fredricks, D. A. Gurnett, and E. J. Smith, ISEE 3 wave measurements in the distant geomagnetic tail and boundary layer, *Geophys. Res. Lett.*, *11*, 335, 1984.

Serlemitsos, P., Low-energy electrons in the dark magnetosphere, *J. Geophys. Res.*, *71*, 61, 1966.

Spjeldvik, W. N., and T. A. Fritz, Energetic ion and electron observations of the geomagnetic plasma sheet boundary layer: Three-dimensional results from ISEE 1, *J. Geophys. Res.*, *86*, 2480, 1981.

Swift, D., Numerical simulation of the generation of electrostatic turbulence in the magnetotail, *J. Geophys. Res.*, *86*, 2273, 1981.

Williams, D. J., Energetic ion beams at the edge of the plasma sheet: ISEE 1 observations plus a simple explanatory model, *J. Geophys. Res.*, *86*, 5507, 1981.

Williams, D. J., E. Keppler, T. A. Fritz, B. Wilken, and G. Wibberenz, The ISEE 1 and 2 Medium Energy Particle Experiment, *IEEE Trans. Geosci.*, *GE-16*, 270, 1978.

Young, T. S. T., J. D. Callen, and J. E. McCune, High-frequency electrostatic waves in the magnetosphere, *J. Geophys. Res.*, *78*, 1082, 1973.

K. A. Anderson and R. P. Lin, Space Sciences Laboratory, University of California, Berkeley, CA 94720.

R. R. Anderson, T. E. Eastman, L. A. Frank, D. A. Gurnett, and C. Huang, Physics Department, University of Iowa, Iowa City, IA 52242.

J. Etcheto, Centre de Recherches sur la Physique de l'Environnement, Centre National d'Etudes des Télécommunications, 92131 Issy les Moulineaux, France.

R. J. Fitzenreiter and K. W. Ogilvie, NASA Goddard Space Flight Center, Greenbelt, MD 20771.

A. T. Y. Lui and D. J. Williams, Applied Physics Laboratory, Johns Hopkins University, Laurel, MD 20810.

M. McCarthy and G. K. Parks, Geophysics Program, AK-50, University of Washington, Seattle, WA 98195.

A. Pedersen, Space Science Department, European Space Agency, Noordwijk, The Netherlands.

H. Reme, CESR, BP 4346, 31029 Toulouse, France.

(Received March 12, 1984;
revised May 21, 1984;
accepted June 5, 1984.)